Major Qualifying Project

Sponsored By: SRI International

Empirical Modeling of the Poynting and Kinetic Energy Flux in Earth's Atmosphere

Authors:

Juan Ortega, Yuchen Xu, Mohammed Alhassan

Submitted to:

Dr. Russell Cosgrove (SRI International)

Dr. Hasan Bahcivan (SRI International)

Professor Andrew Klein (Worcester Polytechnic Institute)

DEPARTMENT OF ELECTRICAL AND COMPUTER ENGINEERING

WORCESTER POLYTECHNIC INSTITUTE

WORCESTER, MA 01609

Abstract

Space weather can affect technology in various ways, such as altering long distance radio communication and satellite signals, diminishing the accuracy of compasses, and even destroying electrical powergrids causing blackouts to entire cities. Due to societies' growing dependence on technologies affected, this project studied the Sun and its solar winds in an effort to predict this weather. Using data recorded by the Fast Auroral SnapshoT Explorer satellite, the final product from this project was the creation of empirical models of the Poynting and kinetic energy flux in the Earth's atmosphere. In future work, an analytical model will be fit to these empirical models in order to further study and predict space weather.

Acknowledgements

This project was completed with the help of our mentors from SRI International and advisors from Worcester Polytechnic Institute, whom we would like to acknowledge and give thanks.

We thank Dr. Russell Cosgrove and Dr. Hasan Bahcivan for helping us learn about space and plasma physics, which was not in our field of study prior to this project. We were able to accomplish the goals for this year of the four-year project with the counsel and help received from Dr. Cosgrove and Dr. Bahcivan.

In addition, we would like to note our appreciation towards Professor Andrew Klein and Professor David Finkel for the support and guidance they provided throughout this project. Both professors provided useful and constructive feedback, which helped us progress with this project

Table of Contents

List of Figures

List of Tables

Executive Summary

This project was the third segment of a four-year project, sponsored by SRI International and funded by the National Science Foundation (NSF), researching the effects of space weather in the upper atmosphere via measurements from the Fast Auroral SnapShoT (FAST) Explorer satellite. The purpose of this year's project was to validate the measured data extracted from the FAST satellite by previous years' teams, and create empirical models of the Poynting and kinetic energy flux based on interplanetary parameters. These models will be used to understand the Sun's energy deposits from the Earth's magnetosphere to the thermosphere.

Space weather can be described as conditions in the Sun, the solar winds, and the Earth's atmosphere that can influence space-borne and ground-borne technologies and endanger human life or health [13]. Throughout every year, the Sun barrages the Earth with solar winds and magnetic storms that can alter long distance radio and GPS signals, diminish accuracy of compasses, destroy electric power grids, and even cause homing pigeons to go astray. As society increases its dependence on technology that is affected from this, a key goal of the National Space Weather Program is the creation of General Circulation Models (GCM), or space weather models simulating the global temperature, circulation, and density of the Earth's thermosphere, in an effort to predict this activity. However, in order to model the density and circulation of the thermosphere, it is necessary to know the energy deposits from solar winds, which have thus far not been adequately quantified [33]. There have been previous attempts using electric field models, however, electric field variability prevents the use of these models for quantification of the Poynting and kinetic energy flux [33]. This project addresses this gap by empirically fitting an analytical model directly to the measurements of the energy input derived from the FAST satellite.

This third year continuation project (2012) developed Matlab scripts and functions to work with the 20,000 orbits of preprocessed data from the FAST satellite to create polar plot empirical models of the Poynting flux and kinetic energy flux. This project had three main goals:

Executive Summary

1. Validate the electric and magnetic field data extracted from the FAST satellite by previous projects.
2. Synchronize the FAST satellite data with Interplanetary Magnetic Field data collected from NASA's Omniweb repository.
3. Develop smoothed statistical polar models of the Poynting and kinetic energy flux dependent on the IMF parameters.

The 2011 MQP group, using Satellite Data Tool (SDT) and Interactive Data Language (IDL) routines, preprocessed 20,000 orbits with electric and magnetic field data. According to the previous MQP group (2011), discussion with Dr. James McFadden from UC Berkeley led to the confirmation that the electron and ion kinetic energy flux was correctly calculated, and thus the data did not need further validation [5]. However, there were a number of orbits containing anomalies in the electric and magnetic field. The anomalies included outlier spikes, sinusoidal artifacts, constant offsets, and sporadic offsets; these errors could have been caused by instrument error, miscalculation of the satellite's attitude, or corrupted data. Since the Poynting flux calculations are directly influenced by the electric and magnetic fields, orbits with these errors were either corrected or not included for the statistical models. Due to the many different types of errors and the large dataset being used, an automated correcting process was needed, therefore, a Matlab function was created to correct or disregard orbits that had large constant offsets and corrupt data. However, due to the limitation of previously developed outlier removal functions, orbits with outlier spikes had to be taken out manually on the orbit-to-orbit basis.

Once we established which orbits contained uncompromised data, we synchronized various Interplanetary Magnetic Field (IMF) parameters, such as the magnitude and orientation of the IMF, number density of protons, solar wind velocity, dipole tilt angle, and the AL index. These IMF parameters were obtained from one of NASA's online data repository known as 'Omniweb,' or Omni. Omni's data is the collective IMF data averaged from several satellites normalized to the commonly used coordinate system known as Geocentric Solar Magnetospheric (GSM) coordinate system. Once the IMF parameters were properly synchronized with the FAST data,

we were able to produce polar models of the Poynting and kinetic energy flux dependent on these parameters. These models showed whether there was a correlation between each of these parameters and the Poynting and kinetic energy flux.

Finally, these models were crude in resolution; therefore, a smoothing interpolation technique, known as regularization, was used to interpolate the models of the Poynting and kinetic energy flux. The idea behind regularization is fitting a fine grid over a coarse grid while minimizing the curvature. By using regularization as opposed to other interpolation techniques, the final plot could show some areas of the plot smoother than other areas.

The fourth and final year of this project (2013) will be conducted by Dr. Cosgrove and Dr. Bahcivan, with WPI students if it is deemed necessary, fitting analytical models to the empirical models we created. They will also be testing the modeling products and publishing papers to professional journals and the public. When this four-year project is completed, the final analytical models will be used to drive General Circulation Models.

Chapter 1

Introduction

Humans have always been captivated by the fascinations of the sky known as the auroral lights. Through science and discovery, it has been determined that the cause of auroral lights is the result of the sun bombarding Earth with energy in the form of solar winds. The effects of solar winds have also been linked to rendering electronics useless, interfering with communication and GPS signals and even causing power grid blackouts. The resulting effects of solar winds and space weather in general can be reduced or prevented by studying how the Poynting and kinetic energy flux, the flow of energy from solar winds to the Earth, is affected.

In order to study the causes of the auroral lights further, the National Science Foundation (NSF) sponsored the 'Empirical Modeling of the Poynting and Kinetic Energy Flux' project proposed by SRI International [4]. Previous models of the Poynting and kinetic energy

flux lacked reliability and credibility because they used inaccurate models of electric field to calculate the Poynting flux. Rather than using model-based calculations, this project attempts to solve this issue by using measured electric field, magnetic field, and particle data collected by the Fast Auroral SnapshoT Explorer (FAST) satellite.

The Poynting flux, which cannot be directly measured, can be calculated by perturbations in Earth's magnetic field caused by space weather and the electric field present in the upper layers of Earth's atmosphere, which are measured by the FAST satellite. This project filled the gap left by previous attempts at modeling the Poynting and kinetic energy flux by using real-time measurements. If the data used in calculating the Poynting flux were not valid, then this model would be no improvement and just as lacking in reliability. In order to account for this, the data used to calculate the Poynting flux must be verified.

One of the goals of this project was to validate the data used to produce the Poynting flux models; these models were created by using Poynting flux data of orbits that were present in interplanetary and geophysical parameters, such as a certain altitude ranges, which are used to study and analyze both energy fluxes. The methodology used to study how the Poynting flux varied with various parameters was then applied to the measured data of the kinetic energy flux. This four-year project incorporated the work of students from Worcester Polytechnic Institute (WPI) completing their 'Major Qualifying Project' (MPQ).

1.1 Project Overview

The resulting empirical models of this project are the combined efforts of Dr. Russell Cosgrove and Dr. Hasan Bahcivan, from SRI International, and WPI seniors completing their MQP at SRI International's headquarters in Silicon Valley. The first two years laid the groundwork by creating functions that allowed the analysis of the FAST datasets in Matlab. The preprocessed data was then used to produce empirical models of the Poynting flux. Our group

was the third and possibly final year involving WPI students in this project. We corrected errors in the electric and magnetic field, then recalculated and created empirical models of the Poynting and kinetic energy flux's dependent on spatial and geophysical physical parameters. These polar plots models of the Poynting and kinetic energy flux were smoothed and interpolated via regularization. The results from this project will be made available to the public and used to drive models of the global temperature, circulation, and density of the thermosphere [4].

1.2 Previous Years

The first year's (2010) project members began by visually inspecting and verifying FAST satellite data, then developing and implementing coordinate system transformation algorithms to be able to model the FAST satellite's data downloaded from UC Berkeley's servers. The results of their project were Matlab routines that calculated the Poynting flux for individual FAST satellite orbit samples. The second year's (2011) project group extracted 20,000 orbits of the FAST satellite's raw data and preprocessed it using Satellite Data Tool (SDT) and Interactive Data Language (IDL) routines. They also optimized the Matlab code that was created in the previous year to be able to calculate the Poynting and kinetic energy flux for large batches of the FAST satellite's orbits. The final product consisted of empirical models of the average Poynting flux over a small number of FAST satellite orbit samples.

1.3 Present and Future

As the third year's (2012) project group, we validated the data produced by the Matlab scripts of previous years. There were a large number of orbit samples where the magnetic field and electric field data were invalid or corrupt, thus it was necessary to inspect all the individual orbits in order to find and omit the outliers. In addition to the Matlab routines and functions created by previously, new routines created this year were used to fit analytical models to the empirical models binned by interplanetary and geophysical parameters. Finally, applying a smoothing technique known as regularization, the final models were smoothed to witness the gradual changes. These final smoothed and interpolated empirical models show the Poynting

and kinetic energy flux's dependence on these interplanetary parameters in an effort to predict this behavior.

The fourth and final year (2013) of this project will be conducted by Dr. Cosgrove and Dr. Bahcivan, with WPI students if it is deemed necessary, reviewing the empirical models on the Poynting and kinetic energy flux and publishing the data to professional journals and to the public.

1.4 Sponsor Overview: SRI International

SRI International, founded in 1946, is an independent, non-profit corporation located in Menlo Park, California, the heart of Silicon Valley [1]. Since its inception, SRI International has been committed to the discovery and the application of science and technology contributing to knowledge, commerce, prosperity, and peace. SRI International provides services to U.S and international government agencies, global corporations, startup companies, and other organizations with a broad range of divisions including engineering and systems, policy, information and computing science, biosciences, and physical sciences. During the sixty-six years of innovation and development, SRI International's contributions have significantly influenced the world. They invented the mouse, sent the first internetwork transmission through wireless communication, and set the U.S High-Definition Television Standard, known as HDTV [2]. By 2010, SRI International staffed over 2100 employees worldwide and earned a total revenue of 495 million dollars.

Chapter 2

Background

The background information begins with space weather and its influences on our everyday lives. Throughout every year, the Sun barrages the Earth with magnetic storms and solar winds that can alter long distance radio signals, diminish accuracy of compasses, and destroy electric power grids. As society increases its dependence on technology that is affected from this, the National Space Weather Program is creating general circulation models to be able to predict this activity.

To study these solar storms further, it is important to understand how and where these solar storms occur. From this, we see that the Sun's energy deposits are measureable in Earth's ionosphere, extending from 80 km to beyond 500 km, in the auroral acceleration region near the North and South Poles.

The energy deposits in the Earth's atmosphere are created via solar wind particles traveling along the Earth's magnetic field lines, also known as Poynting flux. Once the particles reach the ionosphere, they are accelerated and turned into kinetic energy via Joule dissipation. These fluxes essentially describe the flow of energy from our Sun into the atmosphere. Therefore, in order to create models of these fluxes, we used data from the Fast Auroral SnapshoT Explorer (FAST) satellite, which was in operation from August 1996 until September 2001, having recorded 20,000 orbits of the electric and magnetic field's data of the Earth. Thus using the perturbations in the electric and magnetic field along with the electron and ion kinetic energy particle data measured by the FAST satellite, we calculated and created empirical models for the Poynting and kinetic energy flux.

In order to study the cause and effect of the Poynting and kinetic energy flux, the orbits were binned by previous students according to the geophysical parameters, such as the altitude, Invariant Latitude (ILAT), and Magnetic Local Time (MLT). Adding to those geophysical

Parameters, orbits used this year were also binned by the Interplanetary Magnetic Field (IMF) parameters. Binning the data from the FAST satellite by these parameters could give a greater insight as to how the Poynting and kinetic energy flux is affected by the Sun's magnetic field. For example, when the Earth and Sun's magnetic fields connect could show a larger magnitude Poynting flux.

2.1 Space Weather Effects

According to the Solar and Heliospheric Observatory project, the term 'Space Weather' is referred to as, "conditions on the Sun and in the solar wind, magnetosphere, ionosphere and thermosphere that can influence the performance and reliability of space-borne and ground-based technological systems and can endanger human life or health [13]." Like weather on Earth, space weather varies in different forms and strengths. Solar winds and magnetic storms, which normally originate from the Sun, can alter long distance radio and GPS signals [25]. The magnetic storms can also diminish accuracy of compasses, and even cause homing pigeons to lose their way. Finally, these storms can also induce electric currents that can destroy electrical power grids. Since many of these systems govern our lives, and we have grown a dependence on these advanced technologies, it would be useful to be able to predict this weather in order to prepare for it.

The National Space Weather Program is developing a prediction system, using General Circulation Models (GCMs), which are physics-based space weather models that attempt to describe the global temperature, circulation, and density of the thermosphere [5]. However, in order to model the density and circulation of the thermosphere, it is necessary to know the energy deposits from solar winds, which have thus far not been adequately quantified [33]. There have been previous attempts using electric field models; however, electric field variability prevents the use of these models for quantification of the Poynting flux [33]. This project attempts to solve this issue by fitting analytical models to empirical models directly to measurements of the energy input derived from the FAST satellite. The models that this project produces are needed to fuel the GCMs.

2.2 Earth's Atmosphere

In order to understand where majority of space weather activity occurs, we must look at the layers of the atmosphere, specifically the ionosphere. The activity being modeled is energy transferring from the magnetosphere to the thermosphere, which is visible in the ionosphere. The energy arriving from the magnetosphere is mostly in the form of Poynting flux traveling along magnetic field lines, which is partially converted to kinetic energy in the auroral acceleration region [27].

The atmosphere is a collection of gases that surround Earth, held together by its gravity. Divided into five layers, the atmosphere is identified using thermal characteristics, chemical composition, elevation, and density [7]. The five layers, shown in Figure 2.1 below, are the troposphere, stratosphere, mesosphere, thermosphere, and the exosphere.

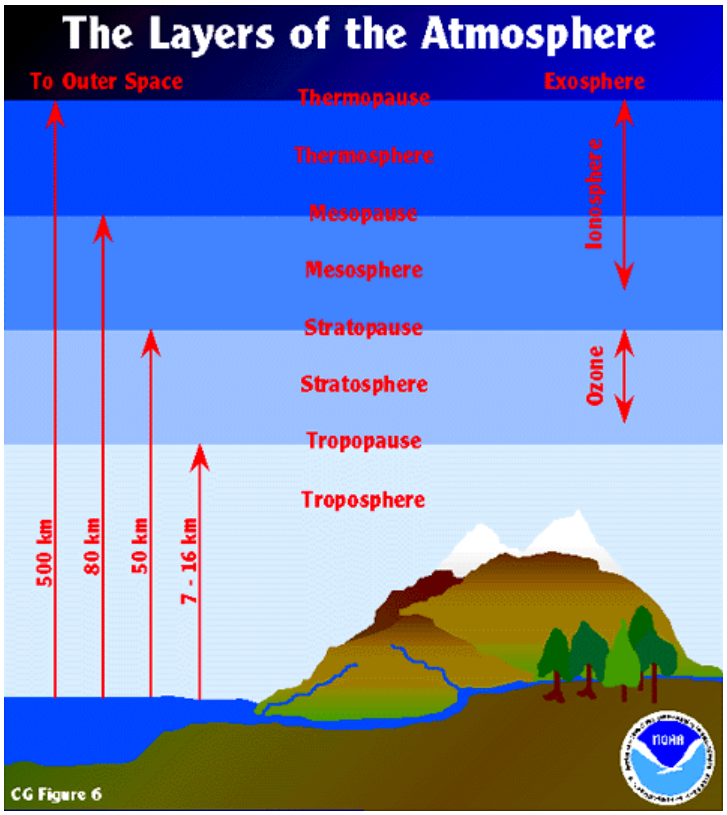

Figure 2.1 – Layers of Earth's atmosphere [26]

Moving higher through the atmospheric layers, the gases become increasingly obscure. At heights of 80 km, inside the mesosphere, the air is so thin that free electrons exist for short

periods before they are captured by a nearby positive ion; this marks the beginning of the ionosphere [8]. The ionosphere extends from an altitude of 80 km to beyond 500 km, comprising the mesosphere, thermosphere, and the exosphere. Most of the ionosphere is electrically neutral, but when solar radiation strikes the chemical components of the atmosphere, electrons can be dislodged from molecules to produce what is known as "ionospheric plasma" [9]. In the ionosphere, ions and free electrons exist in enough quantities such that electromagnetic waves can be reflected and refracted [10]. Thus, the ionosphere plays a crucial role in long distance radio communications as well as absorbing large amounts of solar radiation. The ionosphere is where the FAST satellite measured energy inputs from the Sun.

Above the ionosphere, lies the magnetosphere, a region that is formed when a stream of charged particles, such as solar winds, interact with and are deflected by the magnetic field of the Earth [11]. The shape of Earth's magnetosphere is a direct result of being blasted by solar wind particles. As can be seen in Figure 2.2 below, solar winds give the magnetosphere a tail-like shape that stretches beyond Earth. Although Earth's magnetic field blocks most of the solar wind particles, some leak through the magnetic barrier and are trapped inside. Once inside, particles create an electric field as they travel along Earth's magnetic field lines, in which the cross product is the Poynting flux. When the particles finally reach the ionosphere, they accelerate and produce heat, or kinetic energy, via Joule dissipation in the region known as the auroral acceleration region [27]. Solar wind particles also rush through the funnel-like openings along the magnetic field lines at the North and South Poles, where, once the particles reach the atmosphere, a tremendous amount of energy is released causing the gas molecules to release photons [12].

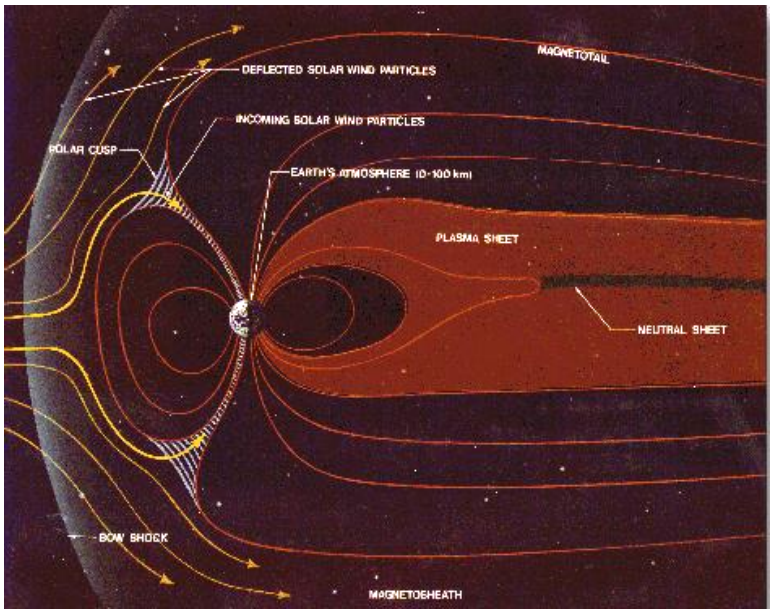

Figure 2.2 – Scientist's map of the magnetosphere [12]

2.3 Poynting and Kinetic Energy Flux

The Poynting and kinetic energy flux are results to the interaction between solar winds and Earth's upper atmosphere layers. The Poynting flux is a vector that describes the magnitude and direction of the flow of energy of electromagnetic waves as they propagate. The Poynting vector is not measured directly; it is the cross product of the measured electric and magnetic fields using the equation:

$$\hat{P}\left(\frac{W}{m^2}\right) = \frac{1}{\mu_0} \bullet \vec{E}\mathrm{x}\vec{B} \qquad (01)$$

The resulting orthogonal vector is the Poynting flux, which in a classical circuit, is the current flowing through a wire in the presence of magnetic and electric fields as shown in Figure 2.3 below.

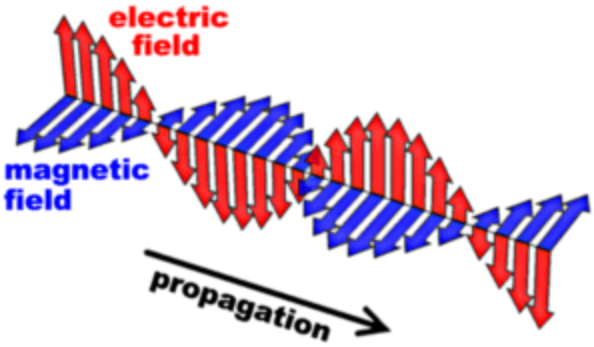

Figure 2.3 – Propagation of the Poynting flux [35].

The kinetic energy flux is describes the flow of particles that absorb energy from the Poynting flux and are rapidly accelerated, emitting heat in the ionosphere. This interaction in the upper atmospheres and the auroral acceleration regions causes particles and ions to be accelerated. The ionospheric plasma mentioned in Section 2.2 is a crucial factor in the transformation from Poynting flux to kinetic energy flux [4].

Quantifying weather in the upper atmosphere is essentially measuring these fluxes of energy. The Poynting flux gives us a magnitude and direction of the flow of energy, as found from Equation (01). Furthermore, the kinetic energy vector tells us the transformation of Poynting flux into moving energy associated with accelerated ions and particles. Sometimes the effects of these energy vectors can be seen as the auroral lights mentioned in Chapter 1.

2.4 FAST Satellite

In order to create empirical models of Poynting and kinetic energy flux, we analyzed the data collected by the FAST satellite, the second mission of NASA's Small Explorer Satellite Program (SMEX). FAST satellite was designed to study the causes and makeup of the aurora, and had assisted the scientists examining the microphysics of space plasma and the accelerated particles around the Earth. In this section, we will introduce the orbit, significant components, and scientific instruments of FAST satellite as well as how the data was collected and transmitted to the Earth.

2.4.1 About FAST

The FAST satellite was launched on August 21, 1996 by the Pegasus-XI rocket [14]. It was sent into an 83-degree elliptical orbit, whose apogee altitude and perigee altitude were 4157

km and 350 km, respectively [15]. Thus, it is possible to observe the particles that generate the visible aurora in the upper atmosphere. When orbiting Earth, the FAST satellite collected high-resolution data, known as 'Snapshots' only in the auroral zones, shown in Figure 2.4 below. The scope of this project consisted of 20,000 orbits spanning from FAST's launch date up to September 2001.

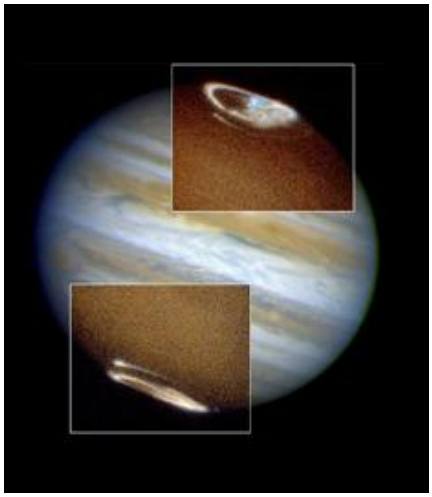

Figure 2.4 – Auroral Regions in Northern and Southern Poles [15]

The satellite has a cylindrical shape, with a base diameter of 1.02 meters and height of 0.98 meters [15]. Together with the 51 kg of scientific instruments, the FAST satellite has a total weight of 191 kg. Within the spacecraft, there was a flight computer that managed instrument operations, data storage, power supply, and the Mission Unique Electronics system (MUE system) [28]. The MUE system was used for the spacecraft's basic life-support functions, such as attitude control, battery control, and saving functions.

2.4.2 Collecting and Processing Data

The scientific instruments used to collect data on the FAST satellite, as seen in Figure 2.5 are: Electrostatic Analyzer (ESA), Electric Field Sensors (EFS), Time of Flight Energy Angle Mass Spectrometer (TEAMS), DC Flux-gate Magnetometer (FGM), and AC Search Coil Magnetometer (SCM) [29]. These instruments, allowed the FAST satellite to collect specific data about the aurora, such as the electric field, magnetic field, electron mass compositions, and ion mass compositions. The electric and magnetic field measurements were used to calculate the Poynting flux, while electron and ion mass composition measurements were used to calculate

the kinetic energy flux. The FGM and SCM were sensors used to collect data from the magnetic field, while the EFS were used to calculate the electric field data; in addition, the ESA collected data for the electron and ion mass composition. However, some interference of the instruments and inaccurate measurements of the sensors could cause some data collected to be unreliable, and examples of the invalid data will be described in Chapter 3.

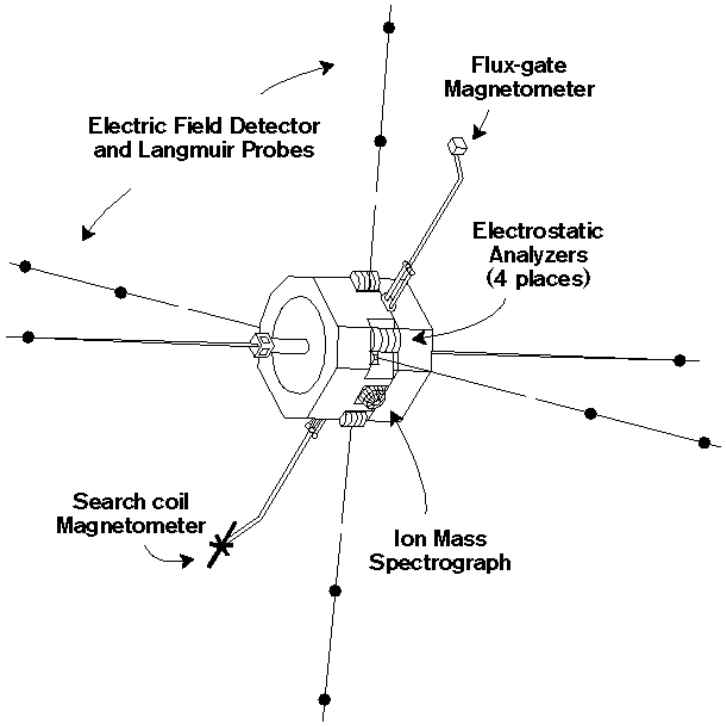

Figure 2.5 – The FAST scientific instruments [5]

Data collected by the FAST satellite was stored on a solid-state recorder [29]. Solid-state memory is quick and reliable when transmitting large blocks of information, such as the "Snapshots". In addition, it is more reliable in harsh conditions than other forms of saving media since it does not rely on moving parts like disks and tapes.

After the spacecraft gathered data, it was telemetered to a ground station, such as the one in Poker Flat, Alaska [30]. Then within a few hours, the raw data was sent to the Goddard Space Flight Center of NASA, in Maryland, where it was packaged and transmitted to the Mission & Science Operations Center (MSOC) at the University of California Berkeley for further study. MSOC constructed a database for the FAST satellite's data, which was collected and simplified by the Satellite Data Tool (SDT). Data that remained too complicated was then

simplified using the Interactive Data Language (IDL). Finally, the analyzed data was extracted and stored into Common Data Format (CDF) files so that scientists could process it easily.

2.5 Geophysical Parameters

From the data measured by the FAST satellite, last year's group was able to compute and produce binned statistical models of the Poynting flux. These models produced were limited to orbits binned by geophysical parameters, such as altitude, Invariant Latitude (ILAT), Magnetic Local Time (MLT), Kp index, and ap index, as described in Table 2-1 below.

Table 2-1 – Geophysical parameters' description

Geophysical Parameters	Description
Altitude	Height from the surface of Earth
Invariant Latitude (ILAT)	Angle from the geomagnetic equator to the geomagnetic North and South Pole
Magnetic Local Time (MLT)	Tells how direct sunlight is along a longitudinal axis.
Kp index & ap index	Measures of geomagnetic activity with respect to time

The ILAT marks the beginning and end of the auroral zone, which is from $\pm 60°$ to $\pm 90°$ for the North and South Poles, respectively. Once the FAST satellite enters the auroral zone, it begins capturing data. The MLT of where the Sun shines directly at Earth also is where the Poynting and kinetic energy flux will be the greatest [5]. The ap and Kp indices are records of geomagnetic disturbances near the auroral regions. These indices are recorded by thirteen substations that average their measurements every three hours [24]. These geophysical parameters allow visual inspection of the dependence between these parameters and the Poynting and kinetic energy flux.

2.6 Interplanetary Magnetic Field (IMF) parameters

The Interplanetary Magnetic Field, or IMF, is a magnetic field emitted from the Sun in all directions. The IMF magnitude and orientation is very important, as any interaction between the IMF and the Earth's magnetic field can affect the Poynting and kinetic energy flux significantly [34]. For example, when the IMF and Earth's magnetic field have opposing

orientations, a phenomenon known as reconnection occurs where the Earth's magnetic field connects with the IMF, allowing any solar wind particles to travel along the connected magnetic fields to enter our atmosphere [27]. The effect of accelerated particles traveling along Earth's magnetic field is explained in the Section 2.1. In contrast, when the IMF and Earth's magnetic field are in the same orientation, there is no significant interaction between them and particles continue traveling along the IMF.

The IMF parameter data used was obtained from one of NASA's online data repositories known as 'Omniweb,' or Omni. Omni is the collective IMF data of several satellites and, unlike the FAST satellite's data; the data from Omni was already normalized to the Geocentric Solar Magnetospheric (GSM) coordinate system.

In addition to the binned statistical model created by last year's group using only geophysical parameters, we incorporated binning by IMF parameters. There were five IMF parameters, as suggested by Weimer's article "An improved model of ionospheric electric potentials," needed to create IMF binning parameters: the magnitude and orientation of the IMF, number density of protons, solar wind velocity, dipole tilt angle, and the AL index, shown in Table 2-2 below [32]. The binning parameters derived from the IMF parameters are explained in Section 3.2a.

Table 2-2 – IMF parameters' descriptions

IMF Parameters	Definition
IMF Magnitude & Orientation	The Y-Z components of the IMF in the GSM coordinate system. IMF Magnitude = $\sqrt{B_y^2 + B_z^2}$. IMF Orientation = $\tan^{-1}(\frac{B_z}{By})$
Number Density	Number of protons per cubic centimeter
Solar Wind Velocity	Velocity at which solar winds are traveling
Dipole Tilt Angle	Angle formed between the geographic North Pole and geomagnetic North Pole
AL Index	Measures of geomagnetic disturbances at high Invariant Latitudes

Chapter 3

Methodology

Figure 3.1 below describes the three main goals of this project. The first goal was to validate the measured data that was extracted from the FAST satellite by previous projects. Once dealing with data that was not compromised, we were able to synchronize the Interplanetary Magnetic Field (IMF) parameters with the time spans for each orbit to create new binned statistical models of the Poynting and kinetic energy flux. When completed, the final task was to apply regularization to these models in order to create a model that is smoother in some areas than others, which when completed, marked the completion of this year's project.

Figure 3.1 – Top level block diagram

There were quite a few orbits, which contained anomalies in the electric and magnetic field data. These anomalies included sinusoidal artifacts, outlier spikes, constant offsets, and corrupted data, which could have been the cause of instrument error, miscalculation of the satellite's attitude, or corrupted data. Since the Poynting flux calculations are directly influenced by both of these fields, to increase accuracy, any orbits that had these errors were either corrected or not included for the binned statistical models.

Once we verified that the data was reliable to use, we then created a function that searched through all valid orbits and created average Poynting and kinetic energy flux models based on orbits that fell into the bins for the chosen parameters. The models were limited by

geophysical and IMF parameters so researchers could analyze and check their relation to specific geophysical events.

Finally, since the models created had values at 30 Invariant Latitude (ILAT) degrees and 24 Magnetic Local Time (MLT) hours, the polar plots originally produced were crude in resolution. Therefore, regularization was applied to interpolate the plots to create a smooth model.

3.1 Validating Data Collected by the FAST Satellite

As mentioned previously, the FAST satellite has collected various types of data, of which we were particularly interested in the following:

Electric Field Data: This data describes the measured electric field for each orbit in the x, y, and z directions.

Total Magnetic Field Data: This data describes the measured magnetic field for each orbit in the x, y, and z directions.

Electron and Ion Particle Data: This data are measurements of the electron and ion particle kinetic energy.

According to the previous MQP group (2011), discussion with Dr. James McFadden from UC Berkeley led to the confirmation that the electron and ion kinetic energy flux was correctly calculated, and thus the data did not need further validation [5]. To complete the first goal of validating electric and magnetic field data, several steps were required. There were 20,000 orbits of preprocessed electric and magnetic field data; however, there were occasions where the magnetic field processing failed. We also observed that some electric field plots had spikes, or artifacts, in them. Therefore, it was necessary to identify orbits with these issues and either fix them or omit them from our models. Since the number of orbits was so large, it was not practical to look through all of the orbit's electric and magnetic field data manually. Therefore, we developed an algorithm to detect these anomalies.

3.1.1 Errors in the Electric Field Data

The electric field data collected by the FAST satellite represented how the electric field had changed at a certain auroral region within a specific period. The magnitude of the electric field in the auroral zone can be influenced by various factors, such as the solar wind velocity, the density of charged particles generated by the solar wind, and the altitude where the electric field took place [34]. According to our orbit data, the magnitude of electric field was relatively small and often centered around zero. However, we found orbits that contained two different types of errors in the electric field data: outlier spikes and sinusoidal artifacts, neither of which reflected valid measurements of the electric field and thus should be modified before used for modeling.

The outlier spike error is considered to be an unexpected significant increase in magnitude within a short period; an example is shown in Figure 3.2, where there is an artifact at 22:47 Universal Time in Orbit 8015. The cause of the spike could have been instability of plasmas near the aurora and could occur in any, x, y, or z, direction of an orbit. The magnitudes of spikes were generally large, and could be more than 700 times larger than normal data in some orbits. In addition, some spikes lasted for more than five minutes and could significantly influence the calculation of the Poynting flux. Thus, in order to create the Poynting flux models accurately, we flagged and replaced significant spikes from the original electric field data with NaNs (Not a Number) in Matlab.

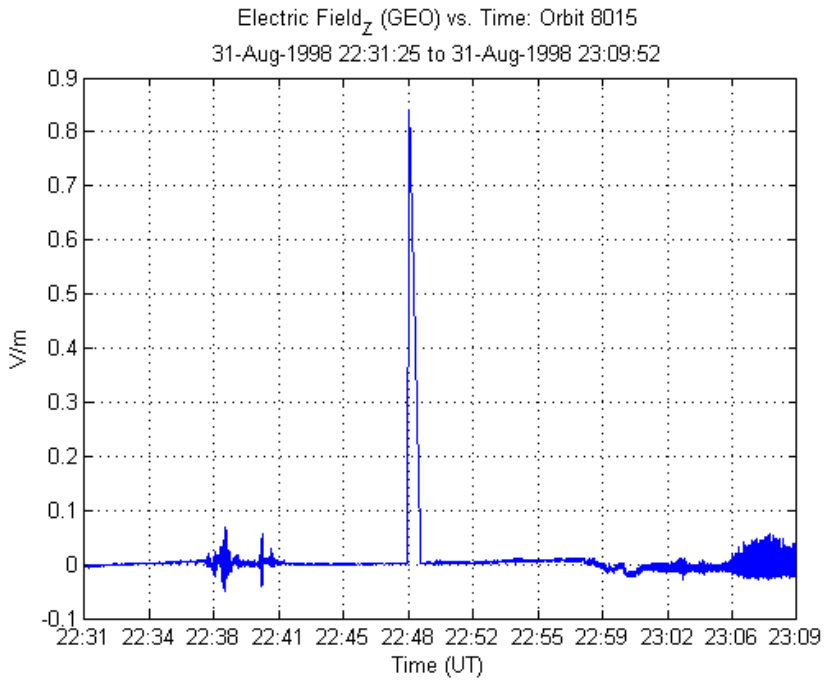

Figure 3.2 – Electric field with spike

The methods we explored to detect spikes in the electric field data of any orbit, in any direction were the Kurtosis Test, Generalized Extreme Studentized Deviate test, and Grubb's Test. These tests share a common idea, which is to propose a null hypothesis that there are no outliers in the data. Then the tests calculated a statistical value based on the samples and compared it with a threshold to decide if the null hypothesis can be rejected. Unfortunately, these tests failed since the electric field data was not a normal distribution as required by said tests. However, after testing over a thousand orbits, we found that orbits that contained spikes had a much larger statistical value γ, calculated as:

$$\gamma = \frac{\text{mean}(|x|) - \text{median}(|x|)}{\text{median}(|x|)}, \qquad (02)$$

where x is the electric field data. Figure 3.3 shows the histogram of γ in all three axes for all the orbits. From this figure, we decided the threshold to be sixty, so any orbit whose γ was greater than the threshold was flagged as an invalid candidate.

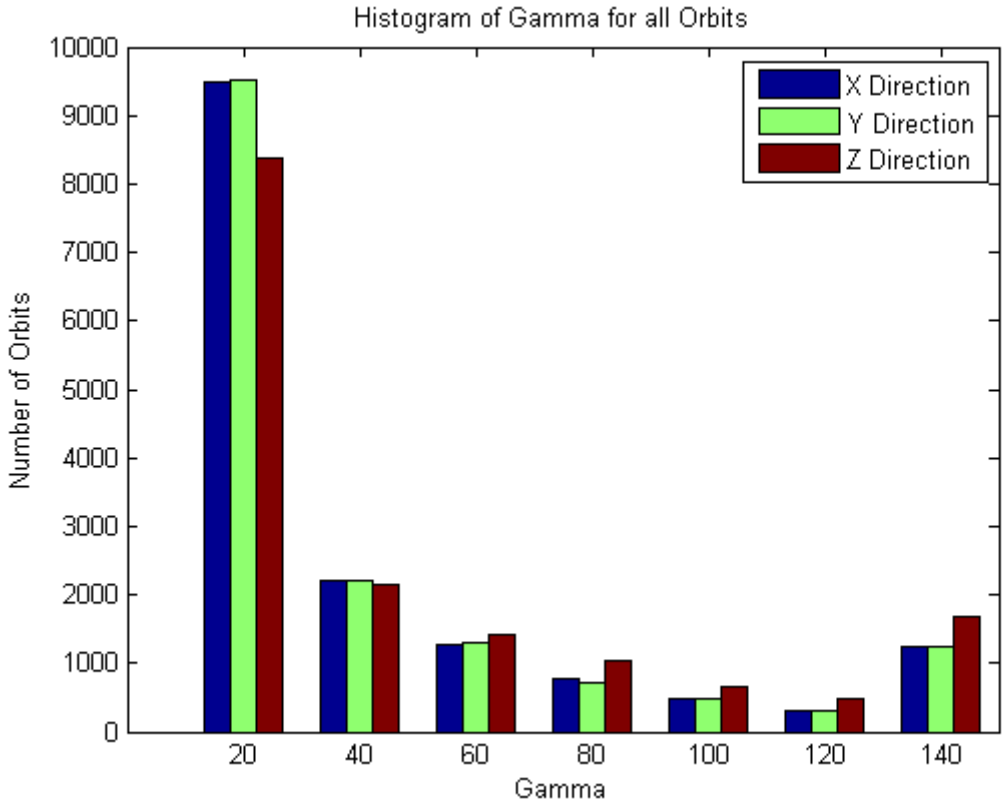

Figure 3.3 – Histogram of gamma values over all orbits with Electric Field Data

In order to remove the spikes in the orbits that were flagged, we first attempted to apply the outlier removal function created by the 2011 MQP group to remove the spike [5]. Unfortunately, this method failed to remove spikes that lasted for a relatively long period and even removed some normal data we wanted to keep. Therefore, we found an alternative method to remove spikes. To do this we manually checked all the flagged orbits, and tried to confirm if there were any spikes, then removed confirmed spikes by replacing the spikes' data with NaN using Matlab. After this method was applied to all the confirmed spikes, data with the removed spikes was saved for future modeling.

The second type of error found within the electric field data was sinusoidal artifacts, such as the one shown in Figure 3.4, and was considered unfixable. Improper unwrapping of satellite's spin axis caused this type of error. In order to detect if there were sinusoidal artifacts, we applied the Lomb Periodogram algorithm to all the orbits. The Lomb Periodogram can

generate the frequency spectrum of the data and the likelihood of a particular frequency occurring, expressed as PN [34]. In our case, we only considered the 0.2 Hz interference produced by the spacecraft. Figure 3.5 shows a histogram of the likelihood of 0.2Hz sinusoidal artifacts occurring over all the orbits. We decided a threshold for PN, δ equaling 150, so that orbits whose PN value surpassed δ were not used for modeling.

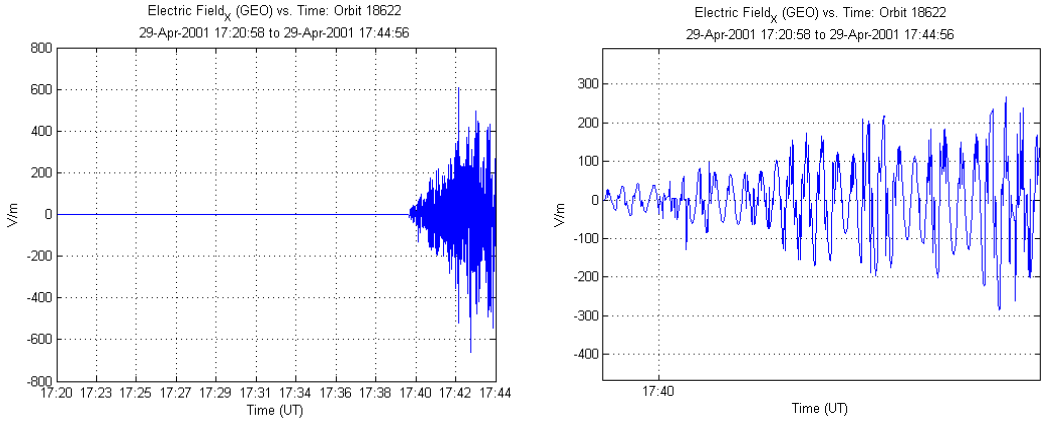

Figure 3.4 – (a) Electric field data with sinusoidal artifacts; (b) Zoomed in sinusoidal artifacts

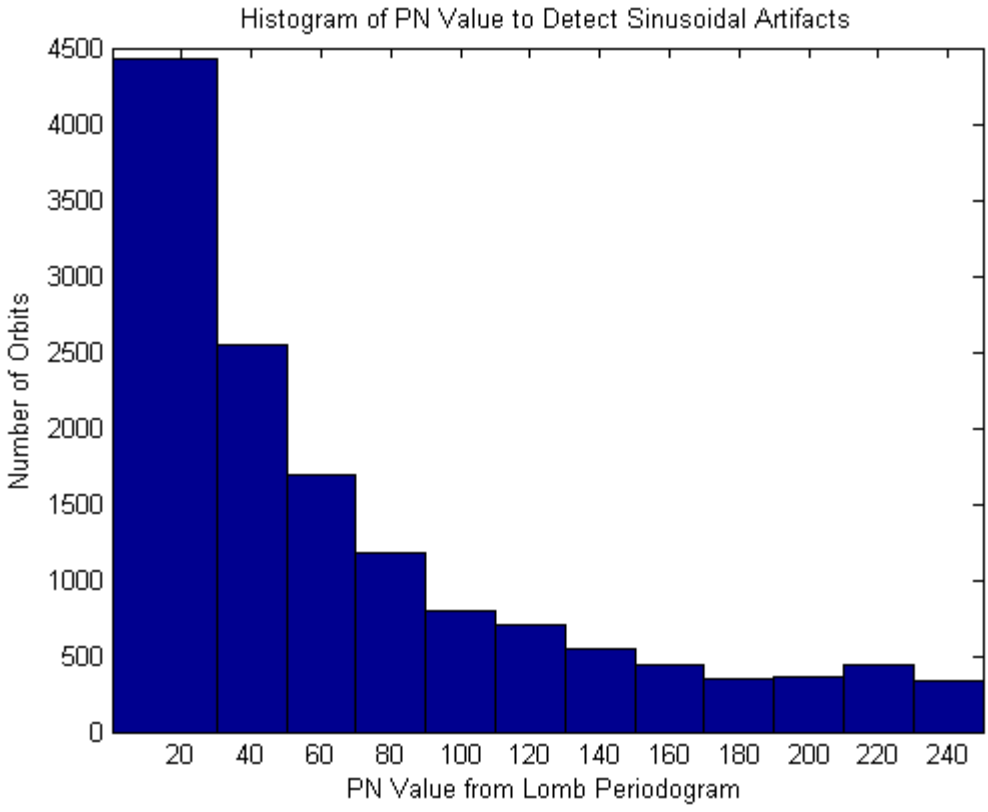

Figure 3.5 – Histogram of Lomb Periodogram for 13904 orbits

3.1.2 Errors in the Magnetic Field Data

The magnetic field plots describe the total measured magnetic field in the x, y, and z directions with respect to the satellite during that particular orbit. However, the Poynting flux is calculated using only the magnetic field perturbations from the Earth's magnetic field, therefore we only cared about the difference between the measured magnetic field and the International Geomagnetic Reference Field (IGRF) model. The IGRF model is an internationally agreed upon model of the Earth's magnetic field that can be used to compare the measured magnetic field. Theoretically, when the measured magnetic field was plotted vs. the IGRF model, both plots should line up except in the period that a geophysical event had occurred from the Sun. These sections of when the magnetic field went astray from the IGRF model are the perturbations we are interested in for the calculation of the Poynting flux. Thus, a new plot was created, delta-B, which is the difference between the measured magnetic field and the IGRF model for the Earth's magnetic field. The delta-B plot should capture the perturbations in the magnetic field.

However, when visually inspecting some of the data, there were orbits found with one of the following three anomalies. The first anomaly is when the total measured magnetic field had a constant offset from the IGRF model as can be seen in Figure 3.6. The second, the magnetic field will have sections of offset glitches as can be seen in Figure 3.7. Third, the magnetic field data was unwound improperly from the spin axis during processing, and thus creating graphs as seen in figure 3.8. A search algorithm was necessary to be able to detect these anomalies so that they were not adding error to the Poynting flux calculations.

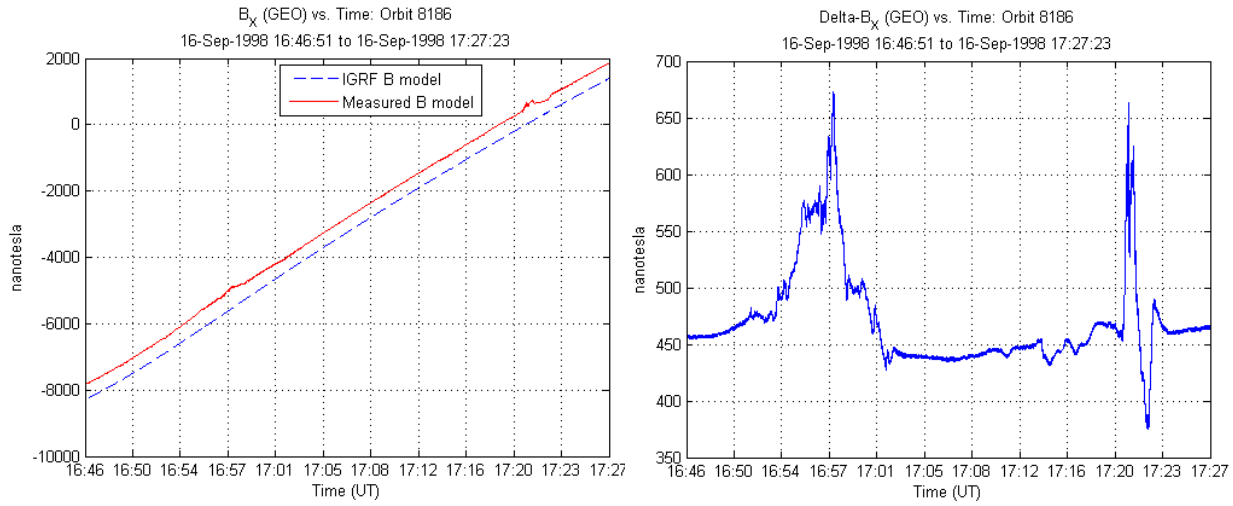

Figure 3.6 – (a) Total magnetic field, and (b) Delta-B magnetic field with offset

The first anomaly could have been due to a miscalculation of the FAST satellite's attitude at the extraction of the data. This particular error was deemed fixable since it appeared that there was a constant offset throughout the data. Therefore, orbits with this issue were fixed by fitting a linear fit to the delta-B graphs, then subtracting that linear fit curve to the total measured magnetic field, which should align the measured data better to the IGRF model. If the absolute value of the delta-B mean increases after applying the linear edge-fitting algorithm, this was probably due to geophysical activity in the edges. Thus the fitting is rejected.

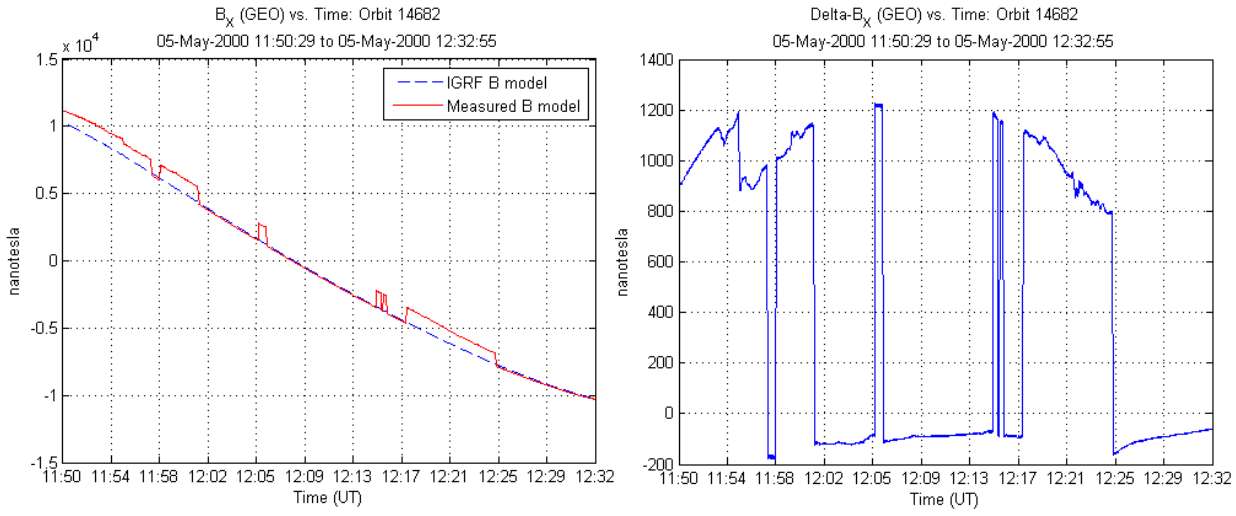

Figure 3.7 – (a) Total magnetic field, and (b) Delta-B magnetic field with glitch offset errors

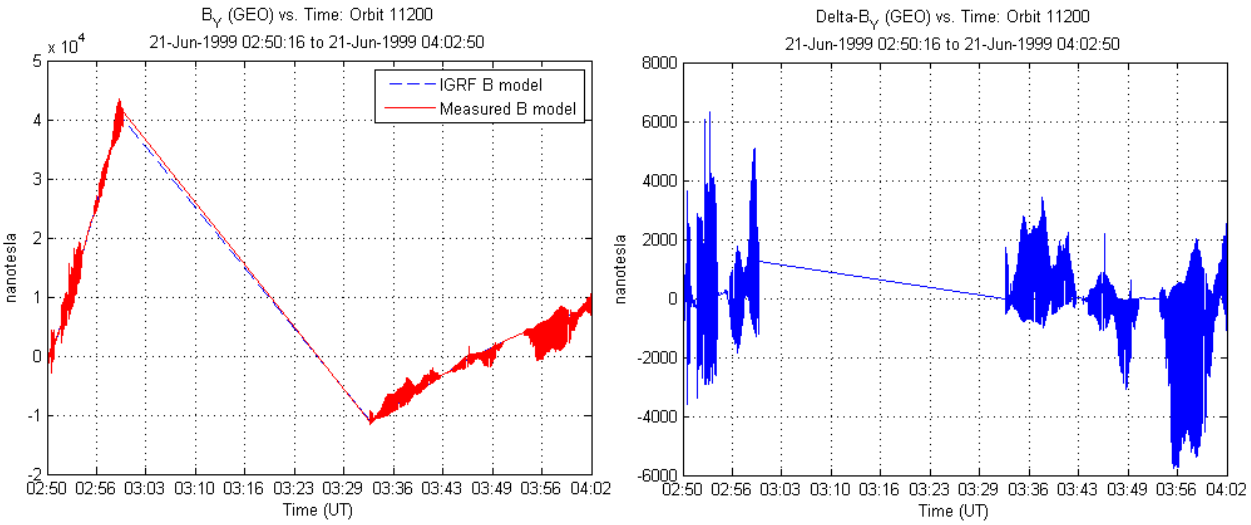

Figure 3.8 – (a) Total magnetic field, and (b) Delta-B magnetic field with spin axis errors

The orbits that had offset glitches or data improperly unwound from the satellite's spin axis were deemed unusable, and corrupted data. Since there were so many differences in the anomalies in the magnetic field, a histogram of the mean values of the delta-B graph was plotted to see how many orbits had large mean values, signifying large offsets. From this histogram, as can be seen in Figure 3.9 below, we see that most of the mean values are centered around 50 nanoteslas. This was good news because it showed that most of the orbits contain good data, and that those with large offsets were few in numbers. Then, starting with orbits with larger mean values, we manually viewed, and categorized these orbits as either good orbits, invalid orbits, or fixable orbits. This method was used to find a threshold of the allowable mean value for the delta-B for which orbits would not have the spin axis error or sporadic offsets, as well as to find orbits with constant offsets, which was fixable. After deciding on a threshold of 200 for the absolute value of the delta-B mean, the linear edge fit algorithm was applied. Thus after completing this long and arduous task, we established a new sample, containing only orbits with "good" magnetic field data.

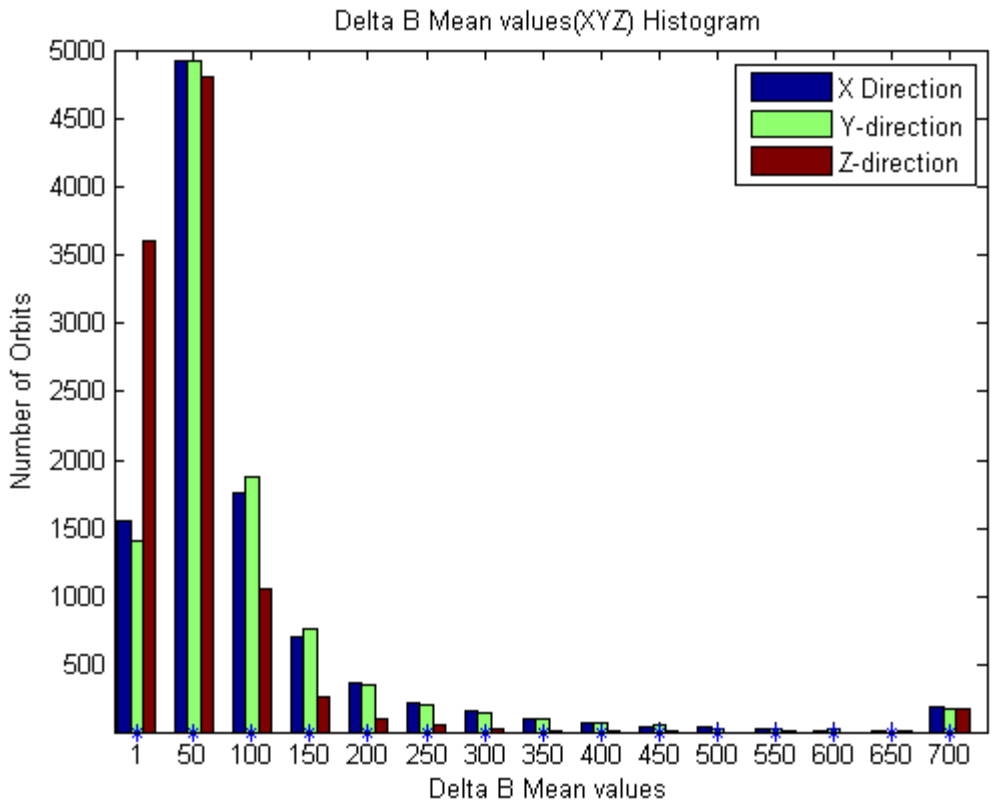

Figure 3.9 – Histogram of mean delta-B values (in nanoteslas) for Orbits 8000-20,000

3.2 Statistical binning of orbits by IMF parameters

Once the data was verified and validated, we were able to create binned statistical models based on IMF parameters. According to Weimer's experience in modeling electric potentials, as described in his article mentioned in Section 2.6, the necessary IMF parameters that were used in his models were the IMF magnitude and orientation, proton density, solar wind velocity, dipole tilt angle, and the AL index [34]. These IMF parameters were used to create the following binning parameters: the IMF's clock angle, the IMF's electric field, IMF's particle momentum, the dipole tilt angle, and the AL index. By binning orbits by certain ranges of these parameters, we were able to see how they affect the Poynting and kinetic energy flux. Before any of the binning parameters were calculated, two propagation delays mentioned in Weimer's article needed to be factored into the equations. According to Weimer, the value of each IMF parameter is affected by up to 20 minutes of its previous values. Therefore, each binning parameter was averaged over the time span of each orbit as well as 20 minutes before the start

of the orbit. The IMF parameter values downloaded from Omni were measured at the bow shock; the outer rim of Earth's magnetic field; therefore, a 10 minute delay was accounted for due to the amount of propagation time to the ionosphere. Thus, each binning parameter value associated with each orbit is an average of the time starting 30 minutes before the beginning of each orbit and ending 10 minutes before the orbit in order to account for both delays. From these measurements, two vectors were created that associated IMF parameters with each orbit. These vectors, discussed in Chapter 4, were used to bin the orbits by the various IMF parameters.

3.2.1 The IMF binning parameters

The first binning parameter, the clock angle, is the resulting angle using the following expression:

$$\tan^{-1}\left(\frac{B_z}{B_y}\right). \quad (03)$$

As mentioned in Section 2.6, these IMF Z and Y coordinates are based on the GSM coordinate system. In spherical coordinates the clock angle, ϕ, is the longitudinal angle coming down from the z to the y plane.

The second binning parameter is the electric field of the IMF calculated by the following expression:

$$B_T^{\frac{2}{3}} \bullet V_{SW}. \quad (04)$$

The solar wind's electric field is typically

$$B_T \bullet V_{SW}, \quad (05)$$

however, as Weimer explains, the electric field value does not increase in a one to one fashion with the IMF, but rather by the IMF raised to 2/3. This parameter allows us to observe how the IMF's electric field affects the resulting Poynting flux i.e. a larger IMF electric field should yield a larger Poynting flux.

The third binning parameter is simply the momentum of particles in the IMF, which is the product of density of protons and the solar wind velocity. This is shown by the expression:

$$n_p \bullet V_{SW}. \quad (06)$$

This parameter allows us to observe how the solar winds add to the kinetic energy flux.

The fourth and fifth binning parameters are the sine of the dipole tilt angle and the AL index. The dipole tilt is the angle formed between the Geographic and Geomagnetic North Poles, the sine of which is unit less. The AL index is similar to the ap and Kp indices in that it measures geomagnetic disturbances; however the AL index has a shorter recording period, making finer data by which to bin. Using the AL index replaced the need to bin by ap or Kp indices.

To inspect how descriptive each IMF parameter is to the Poynting and kinetic energy flux, we created empirical models of the Poynting and kinetic energy flux for each parameter. Orbits were sorted into bins based on ranges in IMF parameters such that each bin contained similar amounts of orbits. These bins are described in Section 4.4.2. Then, we looked for a correlation between an increasing IMF parameter value and the resulting Poynting and kinetic energy flux from the orbits contained in that bin.

3.3 Regularization

From the models generated by the 2011 MQP group, we found the polar plots were coarse and pixilated. In order to produce smoothed and interpolated models, we applied regularization, a commonly used method that produces approximate solutions for inverse problems [36]. In our case, the result of this method provided us local averages distributed continuously over both Polar Regions.

In order to apply regularization, a fine grid was fitted over the original coarse grid by calculating a finite difference approximation to the curvature and applying the method of Lagrange multipliers, which resulted in a fine and smoothed polar plot. This calculation can be approached by taking the second derivative of a cell within the coarse grid in both the horizontal and vertical directions with respect to the grid line. Applying regularization in Polar coordinates was more complex than in the Cartesian coordinate system because calculating the second derivative of the radial and angular components in Polar Coordinates was not as simple as the horizontal and vertical components of the Cartesian Coordinates. To apply regularization

in Polar Coordinates, we fitted a fine grid with dimensions of 60×200 over the coarse grid with dimensions of 30×24 . For the fine grid, assume θ is sixty evenly distributed points within the co-ILAT ranging from zero to thirty degrees, the radial component, and φ is the 200 evenly spaced points ranging from zero to 360 degrees within the MLT, the angular component, i.e. $\mathrm{i} = [1,2,3, \ldots ,60]$ and $\mathrm{j} = [1,2,3, \ldots 200]$, so that

$$\theta_i = \frac{\Delta\theta_i}{2} + \sum_{k=1}^{i-1} \Delta\theta_k \quad (07)$$

$$\varphi_j = \sum_{k=1}^{j} \Delta\varphi_k \quad (08)$$

Then we could calculate the second derivative in θ direction:

$$\frac{\partial^2 u}{\partial\theta^2}\Big|_{\theta=\theta_i} = \begin{cases} 2\dfrac{\frac{u_{i+1j}-u_{ij}}{\theta_{i+1}-\theta_i} - \frac{u_{ij}-u_{i-1j}}{\theta_i-\theta_{i-1}}}{\theta_{i+1}-\theta_{i-1}}, & i \neq 1 \\ 2\dfrac{\frac{u_{2j}-u_{1j}}{\theta_2-\theta_1} - \frac{u_{1j}-u_{1j+100}}{2\theta_1}}{\theta_2-\theta_1}, & i = 1 \end{cases} \quad (09)$$

and φ directions,

$$\frac{\partial^2 u}{\partial\varphi^2}\Big|_{\theta=\theta_i} = \frac{u_{ij+1}-2u_{ij}+u_{ij-1}}{\Delta\varphi^2} \quad (10)$$

except when j=0, substitute j = 200. After we produced a matrix Γ, using the second derivative calculation technique mentioned above, we applied the Lagrange multipliers to obtain the solution P that minimized the mean square curvature. To do this, we substituted G, where $G = \Gamma^{\dagger}\Gamma$, to the following functions to calculate P:

$$P = \frac{1}{2} G^{\dagger} M^{\dagger} \lambda, \text{ where} \quad (11)$$

$$\lambda = H^{\dagger} g, \text{ where} \quad (12)$$

$$H = \frac{\sqrt{\varsigma\Lambda}}{\sqrt{\lambda^{\dagger} C \lambda}} C + \frac{1}{2} M G^{\dagger} M^{\dagger}, \quad (13)$$

where C is the diagonal matrix with second derivative coefficients on the diagonal. Then we would have the matrix P that produced the smoothest possible solution with respect to the original Poynting and kinetic energy flux data.

3.4 Introduction to Bessel Functions

Bessel Function could be an alternative way of the regularization method for smoothing and interpolating the binned statistical models we have generated. The method introduced in this section was not applied since we found the results of regularization met our expectation of interpolating models, however, approximating models using Bessel Functions could be a good practice as a comparison to the regularization for future work.

In order to get a smooth function over the cylindrical region, we will need to minimize the error between the Bessel function expansion and our data; to do this, we could try to apply the Bessel functions expansion. The Bessel functions, also known as the three-dimensional cylinder function, are solution for the Bessel deferential equation, a second order ordinary differential equation shown as follows [37]:

$$x^2 \frac{d^2y}{dx^2} + x\frac{dy}{dx} + (x^2 - v^2) = 0.$$

Unlike interpolating models in the polar coordinates using regularization, Bessel function offers a different perspective of interpolating model in the cylindrical coordinates. It is particularly useful in physical situations where cylindrical symmetry occurs, such as cases involve electric field, heat conduction and vibration. The Bessel function has two commonly seen linear independent solutions, both of which are in the forms of finite series; these two forms are the Bessel function of the first kind with order n, which can be formed with gamma functions, shown in the following formula:

$$J_n(x) = \sum_{m=0}^{\infty} \frac{(-1)^m x^{2m+n}}{2^{2m+n} m!\, \Gamma(n+m+1)}$$

and the Bessel function of the second kind with order n, which is expressed in terms of the Bessel function of the first kind, written as

$$N_n(x) = \lim_{m \to n} \frac{J_m(x)\cos(m\pi) - J_{-m}(x)}{\sin(m\pi)}$$

Thus, the general solution of Bessel function can be expressed in the forms of the Bessel function of the first and the second kind, written as

$$G_n(x) = aJ_n(x) + bN_n(x)$$

There is a Bessel function of the third kind, also known as the Hankel function, which is the sum of the real part of the Bessel function of the first kind and the complex part of the Bessel function of the second kind, however, this solution is only considered in specific situations.

$$H_n(x) = J_n(x) + iN_n(x)$$

There are some more useful properties of Bessel function, which can be used as techniques for conducting models. First, for Bessel function, the recurrence relation holds, that is, a Bessel function of higher order can be determined from Bessel functions with lower orders [38]. For example, given the expression of $J_n(x)$ and $J_{n-1}(x)$, $J_{n+1}(x)$ can be expressed as:

$$J_{n+1}(x) = \frac{2n}{x}J_n(x) - J_{n-1}(x)$$

and so does for N_n and H_n.

Another important property of Bessel Functions is the orthogonality. This property gives us the nth component of the general solution of the physical problem:

$$\mathrm{y_n(x)} = \sum_{\mathrm{p=0}}^{\infty} \mathrm{c_{np} J_n(\lambda_{np} \frac{x}{\rho})}$$

where

$$\mathrm{c_{np}} = \frac{\int_0^{\rho} \mathrm{x} f(\mathrm{x}) \mathrm{J_n(\lambda_{np} \frac{x}{\rho})} \mathrm{dx}}{\int_0^{\rho} \mathrm{x(J_n(\lambda_{np} \frac{x}{\rho}))^2 dx}}$$

and *f(x)* is the nonhomogeneous term of the problem.

The topic of Bessel function can be expend and examined more specifically, however due to the time constrains, this report only proposed the possibility of using Bessel function as sum of two-dimensional plane waves in all directions for interpolating models in cylindrical coordinates. The detail performance of Bessel function and the comparison with regularization method could be a possible approach for future work.

Chapter 4

Results

The main goal of our project was to produce empirical models of the Poynting and kinetic energy flux measured in the Earth's atmosphere by the FAST satellite. As mentioned in Chapter 3, there were three main steps in creating empirical models of the Poynting and kinetic energy flux. First, the measured electric and magnetic field data was verified to be free of any offsets or outlier spikes. The kinetic energy flux was deemed correct by last year's MQP (2011) group, as mentioned in section 3.1. Next, all orbits considered to have good data were binned according to the Interplanetary Magnetic Field (IMF) parameters. Finally, after the orbits were binned, the empirical models were created as polar plots, while using regularization to interpolate between the bins to express a smoothed model.

4.1 Results from Validating Magnetic and Electric Field Data

When processing the 20,000 orbits of data that last year's MQP team preprocessed, we found there were some errors in the CDF files in which data was contained. First, due to unforeseen circumstances, some of the CDF files were not created. This could have been due to either invalid data, or no data being recorded for the specific measurement, such as magnetic field, electric field, positional data, or spin axis data. Since all of these types of measurements are necessary for the calculation and modeling of the Poynting and kinetic energy flux, orbits without these CDF files were discarded. The second error found was that some CDF files were created, however, contained no data. Fortunately, orbits with the second error were very few. From the 20,000 orbits, there were approximately 3,164 orbits with errors in, or no existing CDF files. Therefore, to proceed with validating the electric and magnetic field data, we were left to peruse through 16,836 orbits.

From validating the electric and magnetic field data, we obtained data that resembled the actual data measured by the FAST satellite. Since the calculation of the Poynting flux is dependent on the magnetic and electric field, removing errors and modifying invalid data from

these increased the accuracy of our models. At the end, there were approximately 12,000 orbits whose electric field data was valid, and 14,500 orbits whose magnetic field data was ready to use. Since we only considered orbits of which both electric and magnetic field data were valid, we used a total of 11,966 orbits for modeling.

4.1.1 Magnetic Field Data

Based on whether the measured magnetic field data was correct, had an offset, or was too corrupted to be recovered, the orbits with a delta-B mean less than 200, as mentioned in Chapter 3, were categorized. Then corrupted orbits were discarded, while the orbits that appeared to have an offset throughout were corrected by the offset removal algorithm. Despite the fact that this algorithm was normally only necessary on one of the three axes, it corrected the magnetic field data for more than 8,000 orbits. Figure 4.1 below shows an example of the modified data, in which the modified measured total magnetic field data appears to be a better fit with regards to the IGRF model. To be sure orbits were fixed correctly and there were no more errors, the orbits were sorted by their delta-B mean values starting at the highest. These orbits were manually checked until consecutively receiving good magnetic field data for over 500 orbits. After applying the delta-B mean threshold cutoff as well as visually verifying, out of the 16,836 number of orbits that had CDF files, we now had 14,508 orbits with verified good magnetic field data. Now that all magnetic field data was deemed usable, the Poynting flux could be calculated for our models.

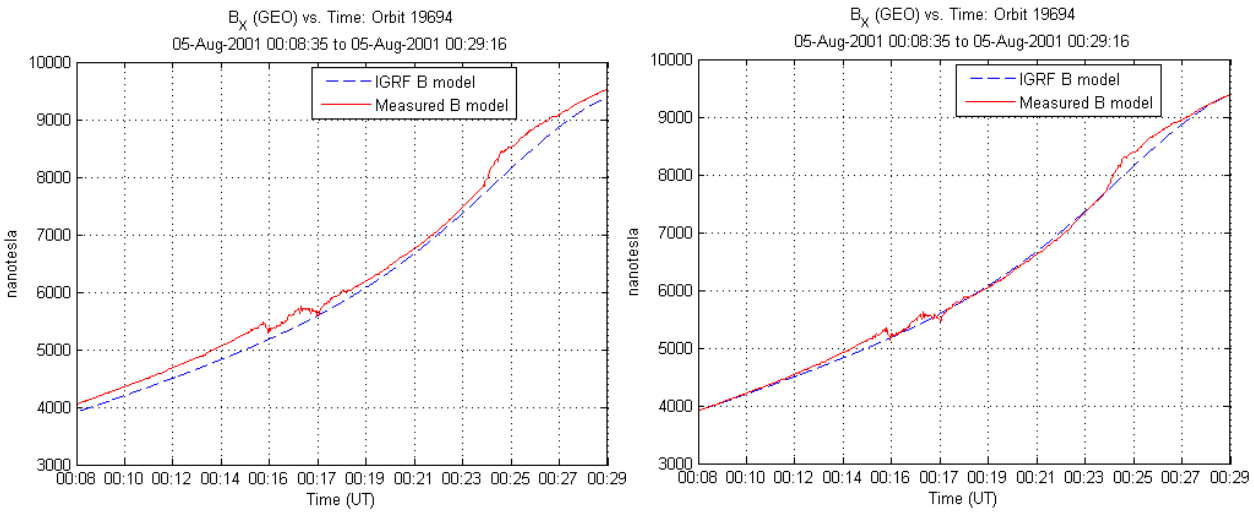

Figure 4.1 – (a) Magnetic field with offset (b) Same data with offset fixed

4.1.2 Electric Field Data

We manually checked 5001 orbits that had been flagged as candidates with invalid electric field data, using the threshold γ equaled 60, as mentioned in Section 3.1.1. The majority of the flagged orbits' electric field data were confirmed to be normal data without any outlier spikes detected; they were flagged because of relatively large electric field magnitudes in certain regions. For the orbits where we found outlier spikes in the electric field data, we attempted to remove their spikes; as an example, Figure 4.2 shows the electric field data of orbit 8015 before and after the spikes removed. As indicated in Figure 4.2.b, the artifact occurring at 22:48 Universal Time no longer exists. In addition, we removed 1798 orbits that contained electric field data with the sinusoidal artifacts that had a frequency of 0.2Hz, the second type of error we mentioned in Section 3.1.1. Thus, the result from validating the electric field data was a collection of approximately 12,000 orbits whose electric field data were spike-free and not significantly influenced by the satellite's spin axis.

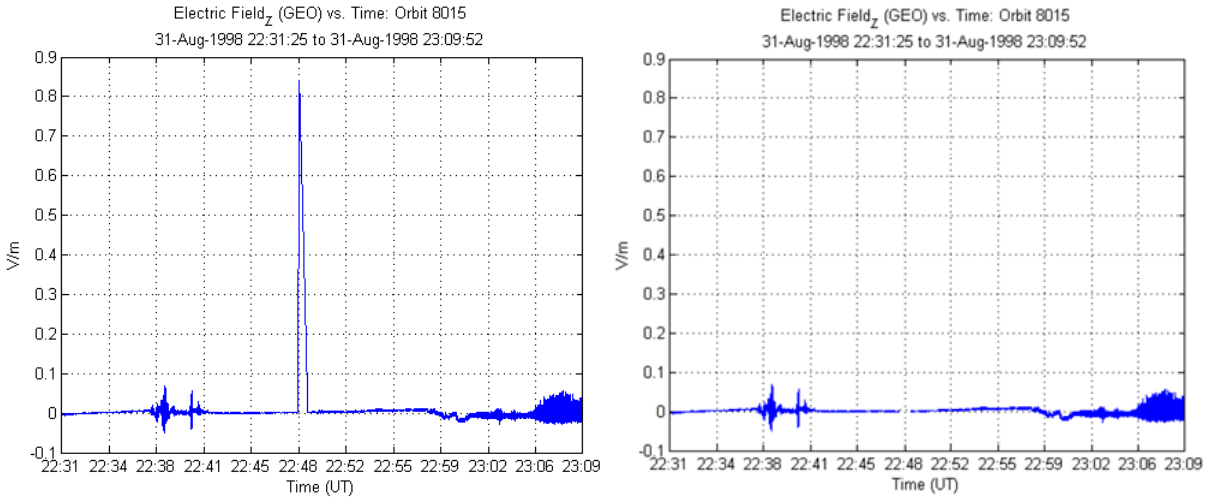

Figure 4.2 – (a) Electric field data with outlier spike; (b) Same data with spike removed

4.2 Remodeling the Total Average Poynting and Kinetic Energy Flux

As soon as the data set was determined to contain accurate data, the Poynting and kinetic energy was recalculated. As mentioned in Section 2.3, the Poynting flux is calculated via the cross product of the electric and magnetic field and divided by the permittivity of free space, as seen by the following equation:

$$\hat{P}\left(\frac{W}{m^2}\right) = \frac{1}{\mu_0} \bullet \vec{E}\mathrm{x}\vec{B} \qquad (01)$$

This process was accomplished for each orbit, and then the Poynting flux was averaged for each of the24 magnetic local times and in each of the 30 invariant latitude degrees. Following this, all the orbits were averaged together to find the average Poynting flux over all the orbits. In order to inspect if the data was correct, we plotted the average Poynting flux for all orbits. Figure 4.3(a) is the average Poynting flux over the Northern Hemisphere, which has plausible data, showing that most activity is occurring around 16:00 Magnetic Local Time (MLT), and around 70 degrees Invariant Latitude (ILAT). In addition, for statistical accuracy, the number of samples used for calculating the average Poynting flux was plotted as well in Figure 4.3(b), which shows that there were over one million samples at almost every MLT and ILAT combination

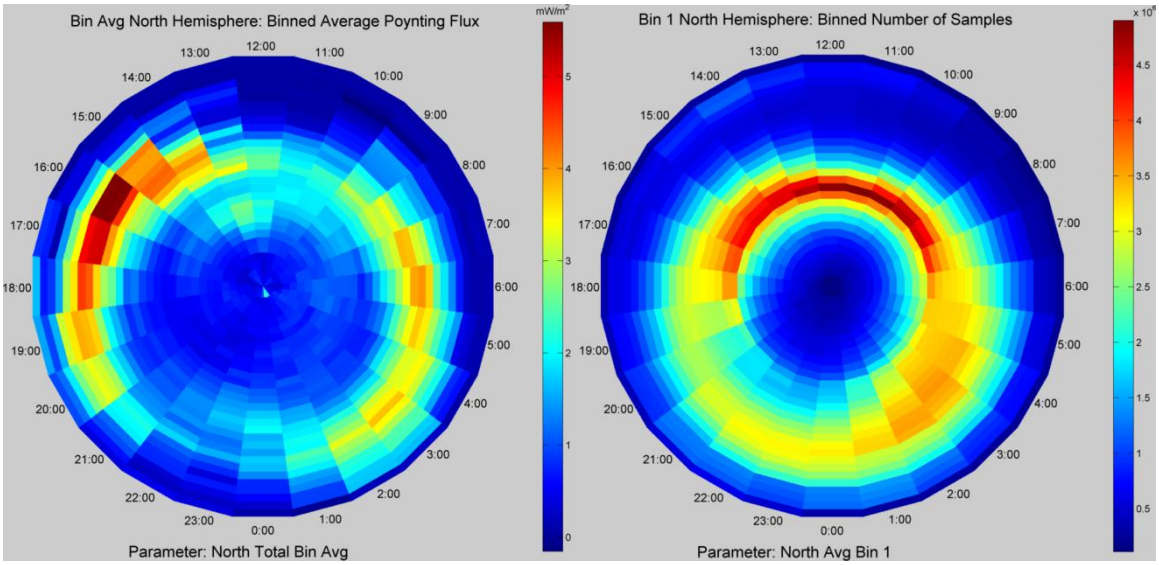

Figure 4.3 – (a) North Hemisphere average Poynting flux (b) Number of samples

Following the modeling of the average Poynting flux, the same procedure was done for the kinetic energy flux. The kinetic energy was simply calculated by adding the measured ion and electron kinetic energies for each MLT and ILAT combinations. The average kinetic energy flux as well the numbers of samples are shown in Figure 4.4 below.

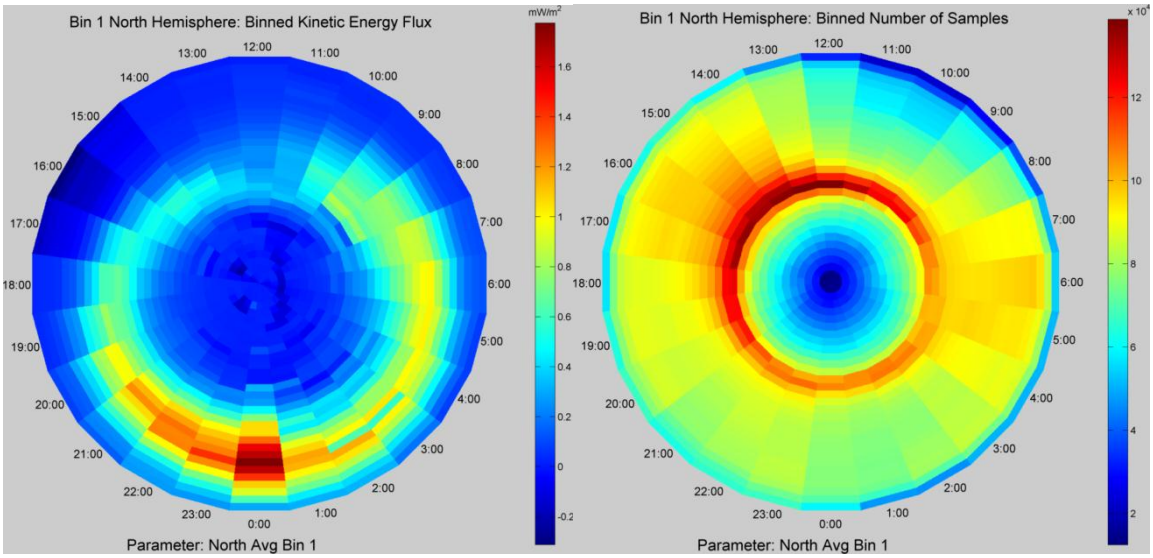

Figure 4.4 – (a) Kinetic energy flux average (b) Number of samples

4.3 IMF Parameter Vectors

A stepping-stone in creating binned statistical models was to create vectors containing IMF parameters mentioned in the methodology. Due to the fact that the majority of the data

from the FAST satellite were half orbits, meaning it only contained values in either the Northern or Southern Hemisphere, two vectors containing the parameter data were made: one vector for the Northern and one for the Southern crossings, respectively. After the orbits used for modeling were reduced by lack of CDF files and unfixable magnetic or electric field data, the amount of orbits was further reduced by Omni data, mentioned in Chapter 2, which was invalid. The Omni data, had portions of invalid data, disallowing an IMF parameter to be derived; any orbits that fell within invalid Omni data were omitted from modeling. This dropped the total number of orbits used for modeling from 13,904 to 13,437. Of the 13,437 orbits, there were 9,657 orbits that contained Northern crossings and 6,232 orbits containing Southern crossings.

4.4 Binning by IMF Parameters

The IMF parameter vectors helped create bins by which we could create models. Bins were created for each parameter so that they contained similar amounts of orbits. Modeling the Poynting and kinetic energy flux from orbits contained in each bin was how we empirically tested how descriptive each IMF parameter was. Table 4-1 and Table 4-2 show the ranges of IMF parameters by which the orbits were binned.

Table 4-1 – IMF binning parameters

NORTH		IMF Orientation - Clock Angle Φ (Degrees)			SOUTH				
Bin	Minimum	Median	Maximum	Orbits	Bin	Minimum	Median	Maximum	Orbits
1	-44.91	2.4615	45	1482	1	-45	3.73	45	994
2	0.0612	57.58	89.98	2143	2	0.16	55.78	90	1482
3	45	88.08	134.97	2690	3	45	90.01	134.96	1850
4	90.06	123.43	179.94	2039	4	90	121.25	179.94	1384
5	-135.00	180.00	135	1376	5	-135	180	135	998
6	-135.08	-123.97	-90.01	1962	6	-179.95	-122.34	-90.04	1404
7	-134.89	-93.52	-45.01	2545	7	-134.96	-90.30	-45	1660
8	-89.98	-55.43	-0.14	1949	8	-89.99	-58.02	-0.058	1231
NORTH		IMF's Electric Field (nT*km/s)			SOUTH				
Bin	Minimum	Median	Maximum	Orbits	Bin	Minimum	Median	Maximum	Orbits
1	46.77	606.87	796.19	2697	1	42.07	634.97	814.56	1833
2	606.67	796.17	973.94	2698	2	634.62	814.47	997.36	1834
3	796.19	974.05	1.16e3	2698	3	814.56	997.60	1.21e3	1836
4	973.94	1.16e3	1.45e3	2699	4	997.36	1.21e3	1.53e3	1837
5	1.16e3	1.45e3	1.01e3	2698	5	1.21e3	1.53e3	9.40e3	1834
NORTH		IMF Particle Momentum (Protons/cc•km/s)			SOUTH				
Bin	Minimum	Median	Maximum	Orbits	Bin	Minimum	Median	Maximum	Orbits
1	1.27e4	5.64e5	7.38e5	2697	1	2.32e4	5.29e5	6.98e5	1833
2	5.63e5	7.38e5	9.19e5	2698	2	5.29e5	6.98e5	8.89e5	1834
3	7.38e5	9.19e5	1.15e6	2698	3	6.98e5	8.89e5	1.13e6	1836
4	9.19e5	1.15e6	1.60e6	2699	4	8.89e5	1.13e6	1.66e6	1837
5	1.15e6	1.60e6	1.03e7	2698	5	1.13e6	1.66e6	1.03e7	1834
NORTH		Dipole Tilt Angle (Degrees)			SOUTH				
Bin	Minimum	Median	Maximum	Orbits	Bin	Minimum	Median	Maximum	Orbits
1	-32.29	-21.76	-13.19	2697	1	-32.31	-18.56	-9.29	1833
2	-21.78	-13.19	-4.28	2698	2	-18.59	-9.30	1.19	1834
3	-13.19	-4.27	7.60	2698	3	-9.29	1.14	10.96	1836
4	-4.28	7.60	17.76	2699	4	10182	10.96	19.89	1837
5	7.60	17.76	32.04	2698	5	10.96	19.58	32.06	1834

Table 4-2 – IMF binning parameters cont.

NORTH		AL Index (nanoteslas)						SOUTH	
Bin	Minimum	Median	Maximum	Orbits	Bin	Minimum	Median	Maximum	Orbits
1	-1.24e3	-197.09	-101.9	2697	1	-1.44e3	-228.64	-120.92	1833
2	-197.14	-101.95	-51	2703	2	-228.67	-120.96	-60.82	1834
3	-101.91	-51	-28	2700	3	-120.92	-60.68	-32.64	1837
4	-51	-28	-14.7	2705	4	-60.82	-32.67	-17.4	1837
5	-28	-14.71	16.55	2700	5	-32.64	-17.41	9.55	1834
NORTH		Altitude (Kilometers)						SOUTH	
Bin	Minimum	Median	Maximum	Orbits	Bin	Minimum	Median	Maximum	Orbits
1	347.62	1.07e3	1.94e3	2697	1	364.04	2.27e3	2.89e3	1833
2	1.07e3	1.94e3	2.64e3	2698	2	2.27e3	2.89e3	3.30e3	1834
3	1.94e3	2.64e3	3.32e3	2698	3	2.89e3	3.64e3	3.64e3	1836
4	2.64e3	3.32e3	3.77e3	2699	4	3.30e3	3.64e3	3.84e3	1837
5	3.32e3	3.77e3	4.15e3	2698	5	3.64e3	3.84e3	4.15e3	1834

4.4.1 Empirical Modeling of IMF Parameters

As we mentioned in Chapter 1, the goal of this project was to produce empirical models of the Poynting and kinetic energy flux. Using the Matlab functions we created, the group working on the final year of this project will be able to analyze the Poynting and kinetic energy flux in depth and explain how the Poynting and kinetic energy flux is affected by various geophysical and IMF parameters. Figure 4.5, 4.6, and 4.7 are an example of where there is a correlation between an IMF parameter the resulting model Poynting flux. These figures are of the IMF's electric field. The electric field present in the upper atmosphere is used to calculate the Poynting flux, so it is reasonable to assume there may be a stronger Poynting flux when a higher IMF electric field is present. Correlations like these will be studied in depth next year by Dr. Cosgrove and Dr. Bahcivan.

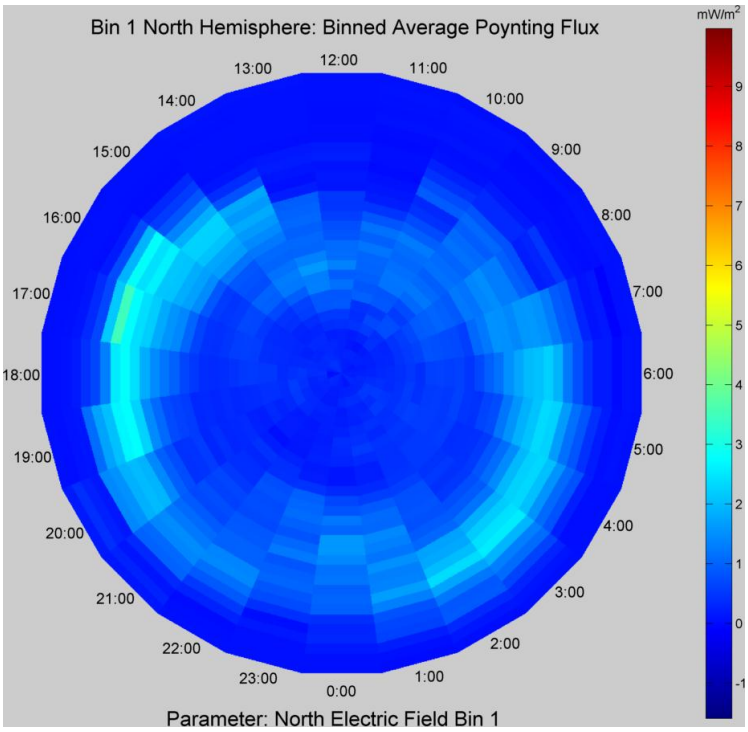

Figure 4.5 – Bin 1 of IMF electric field

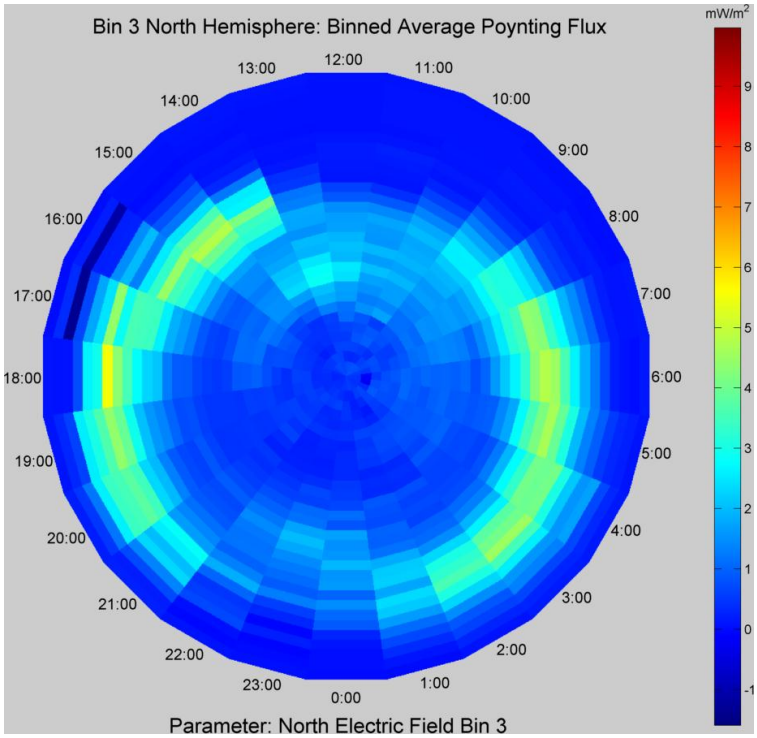

Figure 4.6 – Bin 3 of IMF electric field

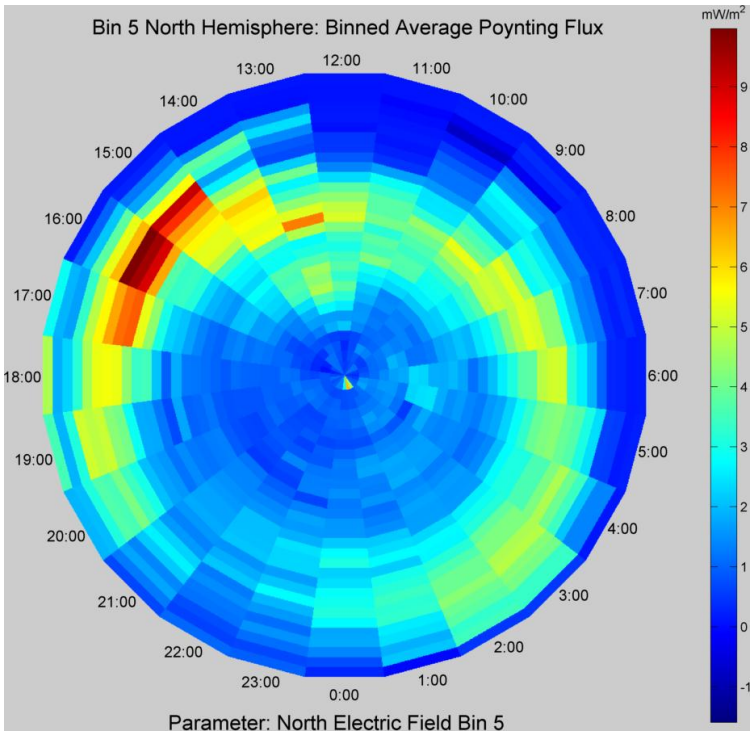

Figure 4.7 – Bin 5 of IMF Electric Field

4.5 Applying Regularization to Polar Plots

After sorting the orbits into the bins for each geophysical parameters listed in Section 3.2.1., we accomplished the main goal of this project, to create models of the average Poynting and kinetic energy flux of the Northern and Southern Hemispheres based on independent geophysical parameters. However, as can be seen in Figure 4.8 below, the original binned polar plots were very crude in resolution, therefore, regularization was applied to smooth and interpolate the data over the polar cap. As a result of using regularization, we can see in Figure 4.9, the interpolated plot has much smoother transactions and displays that some areas are smoother than the others, compared to Figure 4.8.

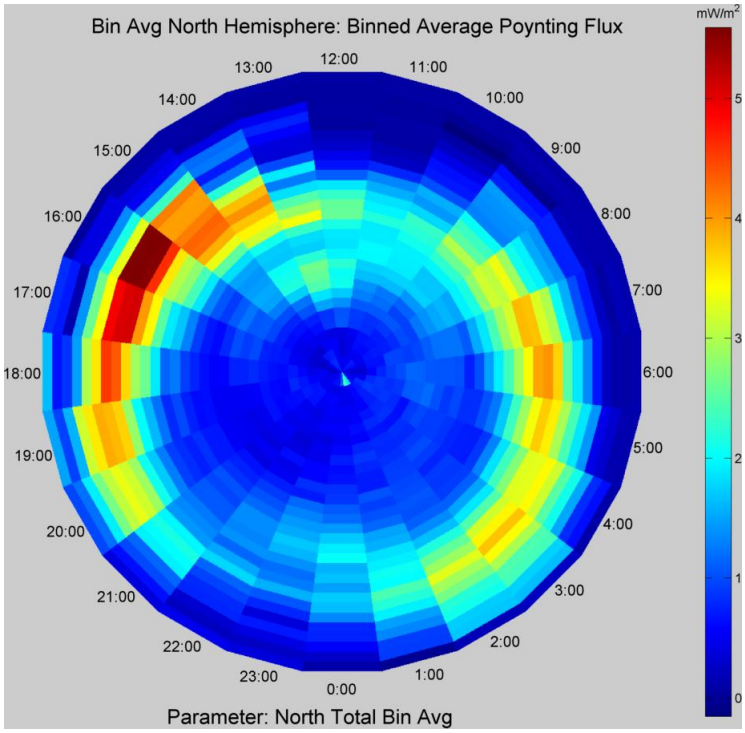

Figure 4.8 – Original, unregularized polar plot

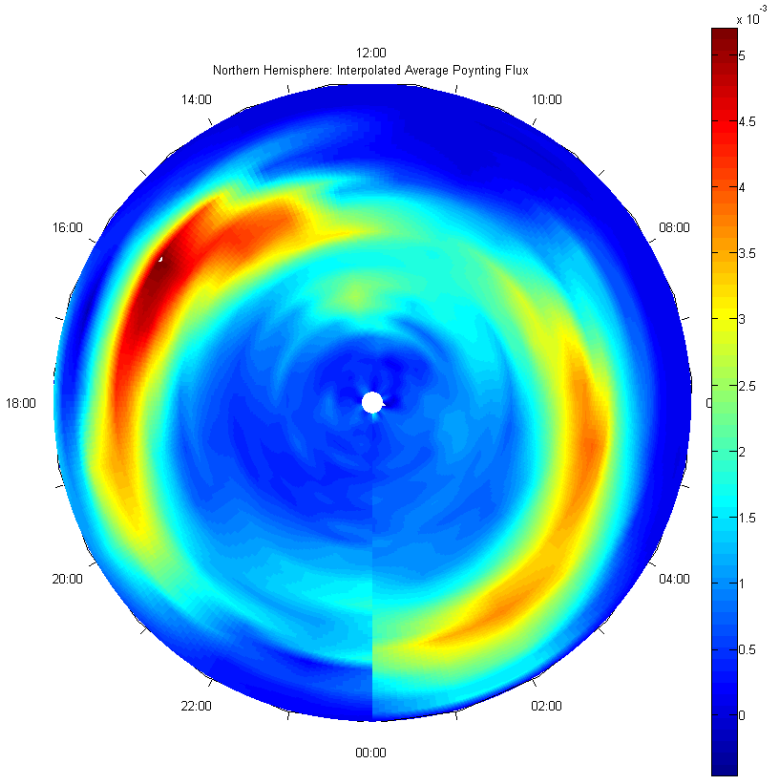

Figure 4.9 – Regularized polar plot

The smoothness of the interpolation plot was determined by the dimension of the grid size. In the examples shown above, we used a grid size of 200x60, which produced a sufficient resolution for our model. In addition, the regularization algorithm can be easily reproduced by increasing the size of the grid to obtain better resolutions. With this algorithm, we were able to minimize the curvature of plots that contained fewer Poynting and kinetic energy flux data averages.

4.6 Summary of Results

The ultimate goal of the third year of this project was to validate the electric and magnetic field data used to calculate the Poynting flux and produce models of the Poynting and kinetic energy flux limited by IMF parameters. The data from the FAST satellite used to produce the models fell from 20,000 to 16,836 orbits due to data being unavailable from Berkeley's FAST data servers. The number of usable orbits then fell to 13,904 when separated from the unfixable magnetic or electric field data. Finally, the number of orbits dropped to 13,437 due to invalid Omni data. Using Matlab, we met our goal to create polar plots for the Poynting and kinetic energy flux models. Then we applied regularization, and obtained more smoothed and interpolated models.

Chapter 5

Conclusion

Space weather is not only the cause of beautiful auroras, but can also cause drastic effects ranging from disabling microelectronics to blacking out an entire city. These consequences motivated governments and scientists to study and predict space weather. Thus the National Science Foundation (NSF) funded this project to produce physics-based space weather models attempting to describe the global temperature, circulation, and density of the thermosphere, or General Circulation Models (GCMs) as mentioned in Chapter 1. In order to create GCMs, models of energy inputs from the Sun to Earth's atmosphere, depicted by the Poynting and kinetic energy flux, are used. Previous attempts to model of the Poynting and kinetic energy flux were insufficient due to the use of unreliable models of the electric field.

This project fitted models to the data collected by the Fast Auroral SnapshoT Explorer (FAST) satellite, thus by using real measured electric field values as opposed to using electric field models we created reliable models of the Poynting and kinetic energy flux. During the first two years of this four-year project seniors from WPI, completing their capstone Major Qualifying Project (MQP), laid the groundwork to analyze the data from the FAST satellite and create Poynting flux models for roughly 3,000 orbits. Our group, the 2012 seniors completing our MQPs, worked to finish the creation of the Poynting and kinetic energy flux models using data from all valid orbits.

First, we validated the electric and magnetic field data used to calculate the Poynting flux. Validating data required creating an algorithm to flag orbits that contained instrumentation or calculation errors. Some orbits that were flagged were considered fixable, thus, the orbits that were flagged, were manually perused and corrected, while those deemed unfixable were omitted from the sample set used for modeling.

Then based on the verified data, we created models of the Poynting and kinetic energy flux limited by the Sun's magnetic field, known as the Interplanetary Magnetic Field (IMF). Using

the IMF parameters associated with each orbit, we created bins, each containing orbits that fell within certain ranges of each IMF parameter. Using the binned orbits data, models of the Poynting and kinetic energy flux were produced; this allowed visual inspection of how the Poynting and kinetic energy flux were dependent on the varying IMF parameter values.

Models of the Poynting and kinetic energy flux from the data contained in each orbit were in the form of polar plots. However, the polar plots of the average Poynting and kinetic energy flux were crude in resolution and very pixelated. Thus one of the goals of this year's project was to employ regularization to make a polar plot smoothed and interpolated between data points. Regularization algorithms in Cartesian coordinates were created in the past; conversely, there has not been much development in polar coordinates. However, with collaboration of Dr. Russell Cosgrove, we managed to apply the same technique in Polar coordinates to produce smoothed plots of the Poynting and kinetic energy flux.

The progress in the final year of this four-year project will consist of analyzing the Poynting and kinetic energy flux data in depth This includes empirically testing how geophysical and IMF parameters, such as altitude and IMF magnitude, affect the Poynting and kinetic energy flux. During this time, SRI International will publish the results of this project to scientific journals for review and then make these models available to the public for any future work.

Authorship

Each of the three project members, Yuchen Xu, Juan Ortega, and Mohammed Alhassan, has contributed to editing this paper. The following table shows the primary author of each section.

References

[1] SRI International. *SRI International about Us* [Online]. Available: http://www.sri.com/about/facts.html.

[2] SRI International. *SRI International Timeline* [Online]. Available: http://www.sri.com/about/timeline/

[3] SRI International. SRI International: Engineering and System Group [Online]. Available: http://www.sri.com/esd/

[4] Division of Atmospheric and Geospace Science of National Science Foundation. *NSWP: Poynting and Kinetic-Energy Flux Derived from the FAST Satellite: an Empirical Model* [Online]. Available: http://www.nsf.gov/awardsearch/showAward.do?AwardNumber=0922230

[5] S. Chen, J. Rehberger, and M. V. Welie, "Automated Processing of Magnetospheric Poynting Flux As Measured by the Fast Auroral SnapshoT Explorer," Worcester Polytechnic Institute, Worcester, MA, 2011.

[6] N. Cahill and S. Musielak, "Poynting Flux And Kinetic Energy Flux Derived from the FAST Satellite," Worcester Polytechnic Institute, Worcester, MA, 2010.

[7] National Weather Service. *Layers of the atmosphere* [Online]. Available: http://www.srh.noaa.gov.ezproxy.wpi.edu/srh/jetstream/atmos/layers.htm.

[8] D. Anderson and T. Fuller-Rowell. (1999). *Space environment topics* [Online]. Available: http://www.swpc.noaa.gov.ezproxy.wpi.edu/info/Iono.pdf.

[9] The High Frequency Active Auroral Research Program. *About the ionosphere* [Online]. Available: http://www.haarp.alaska.edu/haarp/ion1.html.

[10] S.Sorooshyari. Introduction to Mobile Radio Propagation and Characterization of Frequency Bands [Online]. Available: http://www.winlab.rutgers.edu/~narayan/Course/WSID/Lectures02/lect1.pdf

[11] B. Barbier. *The earth's magnetosphere* [Online]. Available: http://helios.gsfc.nasa.gov/magnet.html.

[12] NASA. (1996). *Scientists have drawn a map of the magnetosphere* [Online]. Available: http://xd12srv1.nsstc.nasa.gov/ssl/PAD/sppb/Edu/magnetosphere/mag5.html.

[13] Solar and Heliospheric Observatory. (2011). *Space weather* [Online]. Available: http://sohowww.nascom.nasa.gov/spaceweather/.

[14] University of California Berkeley. *FAST-overview of the FAST mission* [Online]. Available: http://sprg.ssl.berkeley.edu/fast/intro.html.

[15] University of California Berkeley. *FAST Facts* [Online]. Available:

http://sprg.ssl.berkeley.edu/fast/table.html

[16] Anonymous. (1999). *IDL (interactive data language) FAQ* [Online]. Available: http://www.astro.virginia.edu/class/oconnell/astr511/IDLresources/idl-faq-ivsoft-v4.html.

[17] Space Physics Data Facility (SPDF). *CDF-frequently asked questions* [Online]. Available: http://cdf.gsfc.nasa.gov/html/FAQ.html#intro.

[18] E. Thébault, J. J. Schott, M. Mandea, and J. P. Hoffbeck. (2004). *A new proposal for spherical cap harmonics modeling* [Online]. Available: http://www.ipgp.fr/~ethebault/downloads/Thebault%20et%20al_GJI_%202004.pdf.

[19] Wolfram MathWorld. *Spherical harmonic* [Online]. Available: http://mathworld.wolfram.com/SphericalHarmonic.html.

[20] Echo Valley Graphics. *Regularization* [Online]. Available: http://www.pesthomepage.org/PEST_FAQ.php.

[21] Anonymous. Singular value *decomposition* [Online]. Available: http://www.gnu.org/software/gsl/manual/html_node/Singular-Value-Decomposition.html.

[22] Anonymous. *Singular value decomposition* [Online]. 2011(11/22), Available: http://www.uwlax.edu/faculty/will/svd/svd/index.html.

[23] R. Cosgrove, "Empirical modeling of Poynting flux- Year3," Project Description, unpublished, 2011.

[24] Helmholtz Centre Potsdam GFZ German Research Centre for Geosciences. *Geomagnetic ap, Ap, Cp, and C9 Indices* [Online]. Available: http://www-app3.gfz-potsdam.de/kp index/apdescription.html

[25] M. Hapgood and A. Thomson. *SPACE WEATHER: Its impact on Earth and implications for business* [Online]. Available: http://www.lloyds.com/~/media/Lloyds/Reports/360%20Space%20Weather/7311_Lloyds_360_Space%20Weather_03.pdf

[26] Anonymous. *The Layers of the Atmosphere* [Online]. Available: http://www.esrl.noaa.gov/gmd/infodata/lesson_plans/images/CG_Figure_6.gif

[27] M. C. Kelley and R. A. Heelis*, The Earth's Ionosphere: Plasma Physics and Electrodynamics.* California: Academic Press, 1989.

[28]University of California Berkeley*. The FAST Spacecraft* [Online]. Available: http://sprg.ssl.berkeley.edu/fast/sc.html

[29] University of California Berkeley. *FAST Instruments* [Online]. Available:

References

http://sprg.ssl.berkeley.edu/fast/inst.html

[30] University of California Berkeley. *About FAST* [Online]. Available: http://sprg.ssl.berkeley.edu/fast/sc.htmlhttp://cse.ssl.berkeley.edu/fast_epo/discoveries.html

[31] Goddard Space Flight Center. *OmniWeb Plus* [Online]. Available: http://omniweb.gsfc.nasa.gov/

[32] D. R. Weimer, "*An improved model of ionospheric electric potentials including substorn perturbations and application to the Geospace Environment Modeling,*" in *Journal of geophysical research*, vol. *106*, no. *Al*, pp *407-416*.

[33] R. Cosgrove and H. Bahcivan*. NSWP: Poynting and Kinetic-Energy Flux Derived from the FAST Satellite: an Empirical Model* in *National Science Foundation Awards* [Online]. Available: http://www.nsf.gov/awardsearch/showAward.do?AwardNumber=0922230

[34] R. Cosgrove. Personal Communication. February, 2012

[35] University of Leiden. *Light – waves and photons* [Online]. Available: http://www.molphys.leidenuniv.nl/monos/smo/

[36] E.Alpaydin, (2004). *Introduction to machine learning*. Cambridge, Mass: MIT Press. pp*.79,80*.

[37] University of Florida. *Bessel Functions* [Online]. Available: http://www.phys.ufl.edu/~dorsey/phy6346-00/lectures/lect08.pdf

[38] eFunda Inc. *Bessel Differential Equation* [Online]. Available: http://www.efunda.com/math/bessel/bessel.cfm